ELSEVIER

Contents lists available at ScienceDirect

Results in Engineering

journal homepage: www.sciencedirect.com/journal/results-in-engineering





Enhancing the performance of an aerosols-affected solar power tower in arid regions: A case study of wind turbines hybridization

Mohammed S. Alfailakawi ^{a,b,*}, Stavros Michailos ^c, Derek B. Ingham ^a, Kevin J. Hughes ^a, Lin Ma ^a, Mohamed Pourkashanian ^a

- a Energy 2050, Department of Mechanical Engineering, Faculty of Engineering, The University of Sheffield, Sheffield, S3 7RD, United Kingdom
- b Kuwait Ministry of Defense, P.O. Box 1170, Safat, 13012, Kuwait
- ^c School of Engineering, University of Hull, HU6 7RX, United Kingdom

ARTICLE INFO

Keywords: Solar power tower Wind turbine Aerosols Arid climates Water consumption Techno-economics

ABSTRACT

The aim of this research is to investigate the effect of the two most important threats to the solar power towers' (SPT) performance, i.e. aerosols' density and water scarcity, on the SPT feasibility in arid regions. The study is the first attempt to include the site adapted aerosols effect on the SPT's reflected irradiance and comprehensively investigate several new configurations aiming at optimizing the performance and associated costs. Results show that the inclusion of this effect causes an Annual Energy Generation (AEG) reduction of up to 9.1 %. Further, the water consumption analysis is realized based on four different power cycle cooling options, i.e. wet, dry and two hybrid scenarios. Then, a hybridization with Wind Turbines (WT) is proposed as a potential solution to improve the performance of the SPT. The SPT-WT hybridization has been realized with the assistance of an in-house developed algorithm where key design parameters such as solar multiple, thermal energy storage, SPT and WT capacities have been varied over different ranges. It has been found that the configurations with bigger WT share show clear improvements in the Levelized Cost of Energy (LCOE), water consumption and AEG and that's only when the TES is excluded. However, this comes with a penalty on the capacity factor (CF) which witnesses considerable decreases. The results of this study provide new important information that can be used in conceptual engineering studies and inform policy making.

1. Introduction

Solar Power Tower (SPT) has emerged as one of the most promising Concentrated Solar Power (CSP) technologies due to the high sun irradiance concentration levels that it can achieve surpassing all other CSP types [1,2]. Such high levels of concentration are achieved by gathering thousands of flat reflectors, uniquely called heliostats, around a tower top mounted receiver. This results in having an unmatched elevation of the Heat Transfer Fluid (HTF) temperatures to the range of (290–565 °C) [3], i.e. an appropriate working temperature range for the Molten Salt (MS) [4]. This feature enables the technology to deploy the MS as both a HTF and a storage media, which bypasses the need for a heat exchanger between the solar field area and the storage facilities [5], i.e. a common configuration in other CSP types. Also, higher temperatures of the MS in the storage tanks means lower costs as less salt is needed to store an equivalent amount of thermal energy [6].

However, SPT is unique among all other CSP technologies in having its common receiver mounted on top of a tower, which results in having large slant ranges, i.e. the distance between the reflectors and the receiver. This usually reaches thousands of meters and in arid regions, where dust storms are quite frequent, such slant ranges imply a probable amplification of the aerosols effect on the reflected sun irradiance from the reflectors towards the receiver. All other CSP technologies, which have their own receivers within a few meters away from their reflectors, are expected to be much less affected by the aerosols' density on the reflected solar field irradiance. In arid regions, while solar resources are abundant, aerosols high density represents an important obstacle as it is known as the most affecting factor in the attenuation of CSP's main design parameter, i.e. Direct Normal Irradiance (DNI) in cloud free conditions [7–9].

Water scarcity is another aspect of the harsh metrological conditions that can threat the viability of CSP in such regions. The latter affects the

E-mail address: malfailakawi2@sheffield.ac.uk (M.S. Alfailakawi).

^{*} Corresponding author. Energy 2050, Department of Mechanical Engineering, Faculty of Engineering, The University of Sheffield, Sheffield, S3 7RD, United Kingdom.

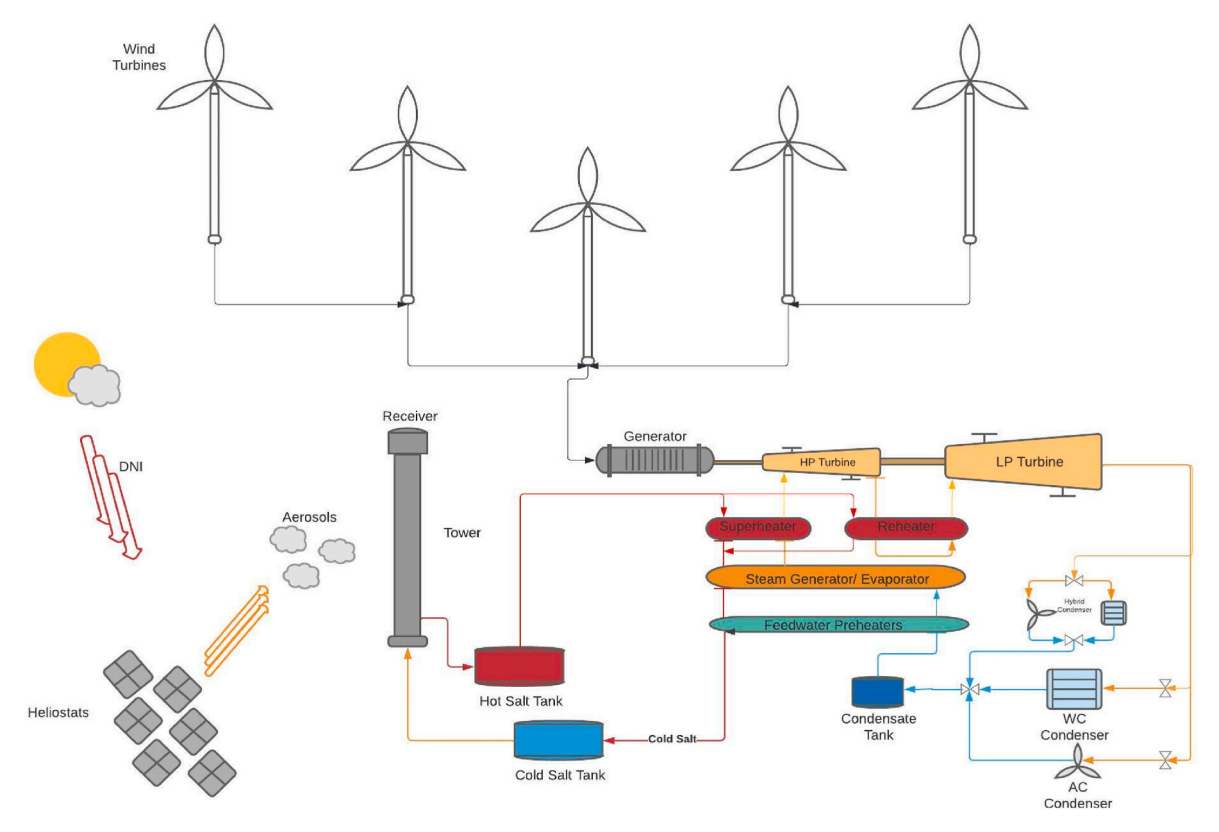


Fig. 1. The hybrid CSP-Wind model based on Solar Power Tower diagram with 3 power block condenser types.

CSP in two different domains, namely reflectors washing and power cycle cooling. Despite being the smaller share in the water consumption (10 % [10]), however, mirror washing cannot be replaced as of yet, as other techniques that discard water usage have not been proven to be as efficient [11]. As for the power cycle cooling process, which consumes most of the water in the CSP, wet cooling condensers remain as the most efficient among other cooling types such as air, due to the higher heat capacitance of water compared to air [12,13]. Water scarcity in arid regions presents another logistical/economical issue as water must be imported from long distances to where CSP should be installed, i.e. where DNI is most elevated and that is usually the driest parts of the region. This is a serious issue for renewable energy application as for example, the Middle East North Africa (MENA) region is known as one among the highest in solar radiation, however, it is also the most water-scarce region in the world [14].

2. Literature review

2.1. SPT and aerosols effect

Aerosols effect on most of the CSP technologies is at best considered in the used weather file, which describes the incoming irradiance among other important metrological parameters. This can be captured as relatively low values of DNI in the weather file. However, the aerosols effect on the reflected irradiance from the reflectors towards the receiver is usually neglected as most CSP receivers are within a very short distance from their respective reflectors. In contrast, the effect of aerosols on the reflected irradiance of the SPT technology is most likely to be big and not to be neglected due to the large slant ranges of the SPT and this cannot be encapsulated in the weather file.

The topic of solar irradiance extinction in SPT plants has been studied since the 1970s when the Vittitoe and Biggs model was introduced and implemented in the DELSOL code for SPT solar fields [15]. However, this model was limited in terms of elevations, atmospheres

and aerosols conditions, therefore its accuracy is limited [16]. Subsequently, this issue has been addressed by developing the Radiative Transfer Models (RTM), e.g. Pitman & Vant-Hull [17], Ballestrin & Marzo [18]. Based on these models, ray-tracing tools have been developed for more accurate solar extinction of the reflected irradiance in the SPT solar field, e.g. HELIOS, MIRVAL and SAM. The substantial improvement in this issue occurs when solar extinction is measured adequately at ground level in Plataforma Solar de Almería-PSA [19] and by using models based on the local AOD parameter and validated with PSA measurements [20]. Among these models, the Polo model [20] is one of the most used. The model includes the effect of aerosols in the DNI attenuation through the integration of the Aerosols Optical Depth (AOD) in addition to the slant range. This model has lead other studies to project the effect of aerosols on the techno-economic aspects of the SPT by different methods, namely: effect on the AEG based on different AOD values [20], and testing the temporal resolution variation effect on the AEG [21].

Despite the fact that the vast majority of the SPT techno-economic studies in arid regions does not include the effect of the aerosols on the reflected irradiance of the solar field [22–26], a previous work of the authors has assessed this effect through a parametric analysis with a variation of the TES and solar field size for a 50 MW SPT in Kuwait [27]. The study examined reported a maximum of 7.7 % decrease in the AEG when considering a daily aerosols resolution effect on the reflected irradiance of the solar field compared to the no-aerosols scenario. All SPT are subject to more or less suffer from the aerosols density in arid regions, and bigger SPT plant capacities, which requires larger solar fields, are likely to suffer more from the aerosols density.

2.2. CSP hybridization

The integration of TES has given a great advantage to CSP technologies enabling them to extend their daily operational hours and thus obtain higher Capacity Factors (CF); CF that can hardly be achieved in

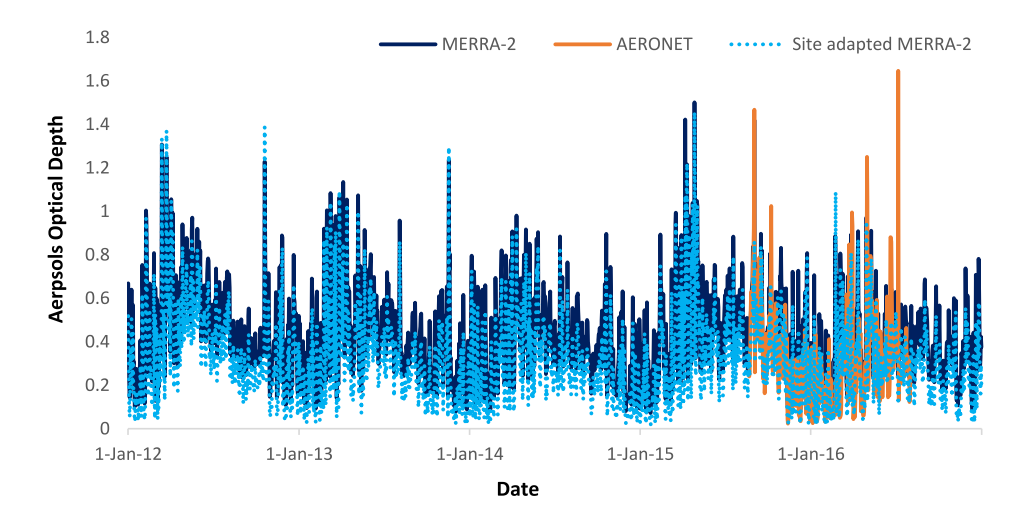


Fig. 2. The site adaptation of 5 years MERRA-2 AOF data with the assistance of 1 year ground measured data of AERONET.

other renewable energy technologies including WT [28]. This has limited the WT in terms of being used as a baseload electricity provider, despite the WT's capability of providing low cost electricity compared to CSP [29]. Hence, a CSP-WT hybridization can be considered viable solution as this configuration can benefit from the WT's decreased LCOE values and the CSP's increased CF.

Thus far, CSP-WT hybridization has been thoroughly studied. For instance, Sahin [30] simulated different capacities of solar and wind after defining the correlation of each technology's potential in the Arabian Peninsula. Similarly, Kost et al. [31] examined different CSP-WT capacities in the MENA region and concluded that the hybrid configuration comes with a lower cost compared to the standalone CSP. Sioshansi and Denholm [32] examined different percentages shares of CSP-WT hybridization fixing the solar field represented by a Solar Multiple (SM) at 1 and varied both the technologies' capacities. The study concluded that a minimum of 67 % share of CSP is required for the hybrid configuration to be economically beneficial. Further, Vick and Moss [33] simulated a 100 MW hybrid model with an alternation of 33 % and 67 % of the CSP-WT shares while fixing the CSP's TES to 6h. They have found that the wind farm with 67 MW and the CSP with 33 MW delivers the best techno-economic outputs.

Despite the large amount of CSP-WT work that exists, the literature still lacks of a work that gradually varies both the solar field size and the TES for different plant capacities along with different capacities of WT. Most of the previous work has focused on the variation of each technology's capacity share disregarding the key design parameters of the CSP, i.e. TES and SM; it is necessary to first optimize these parameters to fully exploit the solar resources by the deployment of a TES. Only then, an optimization of the CSP-WT capacity share can be more accurate and provide more meaningful results. This can be accomplished through a parametric analysis that varies the solar field size paired with a variation of the TES along with the WT hybridization. The importance of such a study lies in the potential of locating a resized solar field-TES configuration for different numbers of WT. The latter will drive the LCOE down, while keeping a threshold for both the CSP capacity and the TES size will ensure that both the AEG and the CF remain at high values. A simplified schematic of the proposed hybrid plant is illustrated in Fig. 1.

The heliostats field reflects the incoming DNI towards the tower top receiver. Then, the HTF passes through the receiver to absorb as much thermal energy as possible from the reflected irradiance. The heated HTF is sent directly to the power block or to the TES for later usage. At the power block, the heated HTF raises steam that enters a typical Rankine cycle, and finally the cold HTF is sent to the cold TES tank. As for the steam, after generating electricity, it is condensed at the

condenser. In this work, three condenser scenarios are considered: air-cooled, water-cooled and hybrid condenser with both air- and water-cooled parts mounted in parallel. The generated energy of the SPT is combined with that of the WT before being exported to the grid.

2.3. Water consumption

Water scarcity is a serious problem in the MENA region in which countries such as the Arabian Gulf are suffering from the lack of both surface and ground water. Kuwait for instance, has negligible surface and ground waters reserves [34]. This water scarcity has a negative effect on the costs of electricity generation as the required process water is provided through Reverse Osmosis of sea water; a relatively energy intensive process [35].

Since CSP emerged as a reliable renewable energy technology, a great deal of attention has been dedicated towards the air-cooled condensers as a reasonable solution for limited water availability for solar applications [36,37]. However, the water-cooled condensers remain as the most efficient cooling type due to its higher heat capacitance, especially in arid regions [38]. In addition, the air-cooled condensers are known for their higher CAPEX compared to these water-cooled ones which can reach up to three folds [39]. On the other hand, the wet cooling option can be an impossible application in some remote arid sites as the water production and transport is too difficult for such locations.

Since water cannot be totally discarded as it is needed for washing the solar field reflectors, therefore, the hybrid cooling option has recently gained an increasing amount of attention; water usage can be limited to the hottest periods of the day/year. Researchers have been keen to observe the hybrid cooling performance with regards to water consumption analysis [40] and AEG [39,41], where it is commonly found that the hybrid option consumes less water compared to the water cooled condenser, however with a penalty in the AEG. Also, the work of El Marazgioui and El Fadar [42] has agreed with previous findings of wet cooling superiority in having higher AEG; however, their work also found that both dry and hybrid condensers have drastically cut down the water consumption. These findings agree with the results of the previous work of the authors [27] which dynamically sized both sides of the hybrid condenser based on the mean dry bulb temperature and thus limited water usage for hot periods of the year.

2.4. Objectives

The main goal of the current work is to assess all the important



Fig. 3. The TAY assembly from the site adapted AOD data (adopted from Ref. [27]).

performance indicators, such as the LCOE, AEG, CF and, especially for arid regions, water consumption in the evaluation process of all the possible configuration of a hybrid SPT-WT plant. The objectives are summarized as follows.

- To set-up and validate the SPT and WT models in the System Advisor Model (SAM) simulation tool.
- To integrate the AOD in the SPT performance model in SAM.
- To hybridize the SPT with different capacities of WT.
- To perform a techno-economic assessment of the hybrid SPT-WT configuration for different TES and SM ranges and different condenser cooling options.

3. Materials and methods

3.1. Metrological data

The metrological data has a great effect on the simulation outputs of the renewable energy technologies. Thus, the accuracy of such data is essential, and the weather file used for the SPT simulation is in the best available form (ground measured data) for the case study location, i.e. Shagaya Renewable Energy Park (SREP) in Kuwait. The weather file is in the form of Typical Metrological Year (TMY) which is basically a long-term data represented by the most typical manner in the form of a single year. This file has been provided by the Kuwait Institute for Scientific Research (KISR) for the benefit of this work.

Despite the TMY's inclusion of the most important weather parameters for a CSP technology, it only describes the incoming irradiance and does not include any parameters that describe the probable attenuation on the reflected irradiance from the reflectors towards the receiver. To do this then the most important factor of this probable attenuation, i.e. aerosols are quantified in this work by an entire year of AOD forming a Typical Aerosols Year (TAY). This TAY is a product of a site adaptation process that takes the advantage of one year of the highest quality ground measured AOD data from the Aerosols Robotic Network (AER-ONET) [43] station in the case study location in addition to a robust five years of AOD data acquired form the Modern-Era Retrospective analysis for Research and Applications Version 2 (MERRA-2) reanalysis model and this is illustrated in Fig. 2.

The inclusion of a multiple year data set is to avoid any short-term data abnormalities that might exist in the one-year ground measured data. It is clear that the AERONET ground measured data used in this work helps in lowering the interpolated AOD values of the MERRA-2 as the 5 years average decreases from 0.429 to 0.326 (dimensionless parameter).

After the site adaptation, a TAY that represents the typical AOD data has been assembled based on the most typical long and short monthly behaviors of AOD over the entire 5 years site adapted period. This has been accomplished with the assistance of the Finkelstein-Schafer statistics (FS) technique which is able to measure the closeness of both the long and short monthly behaviours as follows [19,44]:

$$FS = \frac{1}{N} \sum_{i=1}^{N} |CDF_{m(di)} - CDF_{y,m(di)}|$$

$$(1)$$

where $CDF_{m(di)}$ is the long-term cumulative distribution function of the indices (d_i) daily mean, $CDF_{y,m(di)}$ is the short-term cumulative distribution function in year y and month m and N is the days number in the corresponding month. Once the site adaptation is completed, the TAY assembly is carried out by selecting the months with the closest $CDF_{y,m(di)}$ to the $CDF_{m(di)}$ and thus forming an entire year as shown in Fig. 3 [27].

The TAY results in an AOD yearly average value of 0.3205, which has been used in the atmospheric attenuation function of the SPT in this work as well as the previous work of the authors [27]. It is worth mentioning that no later data of the same quality has been measured by the same station of the case study location which limits this work's ability to use a more recent data. This value is to be integrated in the SPT performance model in the simulation tool used in this work, i.e. SAM. As for the wind resource data, the wind speed and direction among other important metrological parameters for the WT simulation have been acquired form the PVGIS [45].

3.2. System Advisor Model simulation tool

The main simulation tool of this work is the SAM, which is a transient simulation tool that has multiple renewable energy performance models including CSP and WT. The tool approximates a transient system via running a series of steady state solutions over one year period on an hourly resolution. This feature gives accurate hourly outputs which is essential for renewable energy systems due to their intermittent nature. Another substantial advantage of the tool is that it includes both the technical and economic aspects of the simulated technology which permits the user to carry out accurate techno-economic assessments. Also, the tool permits users to import user assembled weather files besides the option of choosing the existing files of the weather library. This is important especially when ground measured data is available as this type of data represents a more accurate input to the tool compared to the widely used satellite data. In addition, the SAM offers a couple of ways to automate the performance models, namely the System Development Kit

(SDK) and the Language Kit (LK). The former enables the user to automate the tool from outside of the simulation core via multiple languages such as C/C++, JAVA, Python, Matlab, while the latter enables the user of automating the SAM from the inside of its simulation core [46].

3.2.1. Solar power tower model

Since the SPT's subcomponents mathematical representations have been thoroughly detailed in the literature [47,48], in this work, only the SPT subcomponents of importance are shown in detail.

3.2.1.1. Solar field. The calculation of the solar field incident thermal energy (Q_{Field}) is carried out by the SAM as follows [49]:

$$Q_{Field} = N_{hel} \cdot A_{hel} \cdot DNI \tag{2}$$

where N_{hel} is the number of heliostats and A_{hel} is the area of a single heliostat in the solar field. The solar field is supposed to entirely reflect the incident thermal energy at the receiver, however, the solar field of the SPT, as do other CSP types, suffers from specific type of losses which define the optical efficiency of the solar field (η_{opt}):

$$\eta_{opt} = \eta_{cos} \cdot \eta_{at} \cdot \eta_{sp} \cdot \eta_{s\&b} \tag{3}$$

where η_{cos} is the cosine loss, η_{at} is the attenuation loss, η_{sp} is the spillage loss, $\eta_{s\&b}$ are the losses due to the shadowing and blocking [50]. The conventional set up in the SAM only considers the distance effect in the attenuation loss η_{at} and that is in the form of a third order polynomial. An introduction of aerosols representative coefficients is necessary in order for the polynomial to include the most important factor in the probable attenuation of the reflected DNI as follows:

$$A(\%) = aS^3 + bS^2 + cS + d \tag{4}$$

The mathematical calculation of the four polynomial coefficients is carried out in this work based on the Polo model [20], which integrates the effect of the aerosols in addition to that of the distance. The Polo model is given as follows:

$$a = 3.13 \text{ AOD}^3 - 1.9 \text{ AOD}^2 + 1.6 \text{ AOD} - 0.133$$

$$b = -14.74 AOD^3 + 2.49 AOD^2 - 11.85 AOD + 0.544$$
 (5)

 $c = 28.32 \ AOD^3 - 7.57 \ AOD^2 + 48.74 \ AOD + 0.371$

$$d = -2.61 \text{ AOD}^3 + 3.70 \text{ AOD}^2 - 2.64 \text{ AOD} + 0.179$$

Eventually, the incident thermal energy that manages to reach the receiver after being affected by the aerosols among the other optical losses of the solar field is calculated as follows [51]:

$$Q_{rec} = A_{hel} \cdot N_{hel} \cdot DNI \cdot \eta_{opt} \tag{6}$$

Also, the relation between the energy delivered from the solar field size and that needed at the power cycle is described by the SM, which is the ratio of the thermal power produced by a specific solar field size at the design point to the power required at the power cycle block at nominal conditions [5]. In other words, a SM of 1 basically represents a solar field size with which the plant should deliver just enough power directly to the power block with no excess power. While a SM of 2 can provide the sufficient power requirement at the power block in addition to an equivalent amount of excessive power (to co-generation or the TES for later usage). The SM can be calculated as follows [52]:

$$SM = \frac{Q_{Field}}{Q_{pb}} \tag{7}$$

where Q_{pb} is the thermal power required at the power block for nominal conditions operation. Also, a variation of the SM is projected at the tower height and thus, a variation of the slant range. The relation between the SM and the tower height can be expressed as follows [53]:

$$h_{SM} = h^* \sqrt{SM} \tag{8}$$

where the h is the tower height for a SM = 1 while the h_{SM} is the tower height at any other specific SM value.

3.2.1.2. Thermal energy storage (TES). In this work, the TES is simply represented by the number of full hours that the storage system can deliver to the power block at its rated capacity. In terms of thermal energy, the amount of energy required for the desired number of full load hours of TES within the designated range can be calculated as follows:

$$Q_{TES} = Q_{HTF} * t_s \tag{9}$$

where t_s is the number of TES full load hours and Q_{HTF} is the required thermal energy to be transferred to the HTF which can be obtained based on the solar field output and the efficiency of the receiver as follows:

$$Q_{HTF} = Q_{rec} * \eta_{rec}$$
 (10)

The receiver efficiency η_{rec} is based on multiple probable losses that the receiver suffers from and is broken down in more detail in the supplementary materials.

Then, in order to store the corresponding volume of molten salt that can store the desired thermal heat in the HTF (Q_{HTF}), the mass of the HTF must be calculated. This can be obtained as follows [54]:

$$m_{HTF} = \frac{Q_{TES}}{C_P^* (T_{hot} - T_{cold})} = \frac{Q_{HTF}^* t_s}{C_P^* (T_{hot} - T_{cold})}$$
(11)

where C_P is specific heat of the molten salt, T_{hot} and T_{cold} are the hot and cold tanks temperatures, respectively. Hence, the volume of the molten salt V_{HTF} is obtained as follows [55]:

$$V_{HTF} = \frac{m_{HTF}}{\rho_{HTF}} \tag{12}$$

where ρ_{HTF} is the HTF density. This eventually shapes the TES tank size (V_{TES}) as follows:

$$V_{TES} = \frac{V_{HTF}}{\eta_{TES}} \tag{13}$$

3.2.1.3. Power block (condenser scenarios). Despite the reported lower performance of the air-cooled condensers in the literature, the latter can sometimes be an obligation rather than an option in arid regions due to water scarcity. On the other hand, a water consumption elimination in the CSP plant is not, as of yet, a solution in the reality as all CSP plants require water to clean the reflectors. Based on the latter, a trade off solution is proposed in this work by the assessment of a hybrid condenser scenario which only consumes water when it is needed. That is avoiding water consumption when the ambient air temperature is low enough to perform as good, or close to, the heat rejection process in the power cycle as the water would do. Thus, when the ambient temperature is high in the summer period, the water-cooled side of the hybrid condenser is activated. This being said, based on the reference ambient temperature a switch takes place from air to water cooling and vice versa.

The dry bulb temperature is considered as the reference temperature in this work as it describes the air temperature. Along with that, it is taken as a measurement for the performance of the air-cooled power cycle as it has been found that beyond certain air temperatures, a clear drop of the efficiency of the air-cooled condenser takes place. In this work, both 32 $^{\circ}$ C and 37 $^{\circ}$ C are taken as reference temperatures for scheduling two hybrid condenser operating strategies as these results have been found to be on the threshold of having a noticeable and a serious efficiency drop, respectively [56].

In an air-cooled based Rankine cycle, the cycle efficiency is a unique

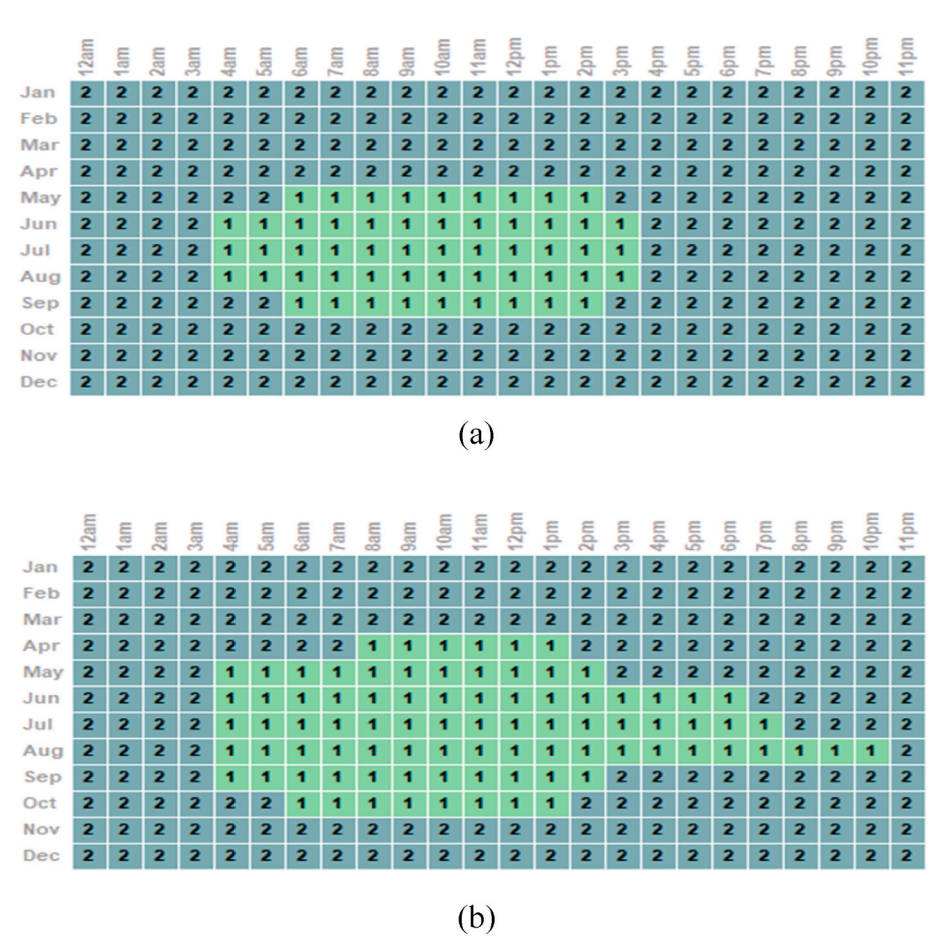


Fig. 4. The SAM hybrid condenser system control for (a) the 19 % hybrid scenario and (b) the 30 % scenario [27].

function of the dry bulb temperature (T_d) and can be obtained as follows [57]:

$$\eta_d = -0.1468 \, T_d + 22.526 \tag{14}$$

On the other hand, in the water-cooled condenser, both the dry bulb temperature and the relative humidity are of importance in the efficiency of the power cycle. This is because the difference between the wet and dry bulb temperatures depends on the humidity in the air (wet and dry bulb temperatures are equal at 100 % humidity [38]). Thus, the water-cooled condenser efficiency is obtained as follows:

$$\eta_{w} = a(\phi)T_{d} + b(\phi) \tag{15}$$

Where ϕ is the relative humidity, and a and b can be obtained as follows:

$$a(\phi) = -0.102 \,\phi - 0.0684 \tag{16}$$

$$b(\phi) = -0.305 \ \phi + 24.26 \tag{17}$$

The SAM enables the user to assign the ambient temperature at design and this is known as the temperature at which the power cycle is supposed to operate at its rated efficiency. For an air-cooled condenser, the ambient temperature at design must be the dry bulb temperature, while conversely it should be the wet bulb temperature in the case of the water-cooled condenser [57,58]. The current work has employed the average wet/dry bulb temperatures from March to September of the weather file as the design temperatures because this period of the year is the period at which CSP is usually expected to deliver its highest production [59].

Consequently, based on the two dry bulb temperatures that have been assigned as the reference for both scenarios in accordance with the dry bulb temperature profile in the used weather file of the case study location, the two hybrid condenser scenarios are set up as follows: 30 % of the annual hours are found to be superior than a dry bulb temperature of 32 °C, thus the water-cooled side of the hybrid condenser is only activated for 30 % of the year time and thus the first hybrid scenario is named accordingly: 30 % hybrid condenser. On the other hand, only 19 % of the year have been found to be superior to 37 °C which insists on activating the water-cooled side and thus the second scenario is named as 19 % hybrid condenser. This has been automated in the SAM for every hour of the day over the entire year as it is illustrated in Fig. 4.

3.2.1.4. SPT model validation. As the SPT is one of the most sensitive and complex CSP technologies, and this is mostly due to the solar field configuration, the simulation in this work is carried out with two steps validation. The first step of the validation is accomplished against data from the commercial SPT of Gemasolar [60] in Sevilla, Spain (see the supplementary materials for more details). This step is carried out to prove the tool's compatibility in simulating real life applications. Further, the second step is carried out only because the required SPT capacity for this work (50 MW) is limited in terms of the available published data from commercial plants of the same capacity. Hence, a validation against a 50 MW SPT simulated published data [61] has been carried out and the results can be found in a previous work of the authors [27]. Both validation steps yielded good agreement as no more than a 5.7 % deviation has been found in the AEG and the CF. A maximum deviation of 8.8 % has been found in the LCOE between this work and the data derived from Ref. [61] and this is most probably due to the different economic parameters used by the authors for their specific

This work's base model inputs have been mainly based on the data from Ref. [61], as it is of a similar plant capacity. However, some specific

Table 1 SPT technical parameters.

	parameter	description
System Design	Solar multiple	1 to 3.8 (with a step of 0.4)
	Irradiation at design	700 W/m ²
	HTF hot temperature	565 °C
	HTF cold temperature	290 °C
	Full load hours of	0-18 (with a step of 3 h)
	storage	
Tower and Receiver	Tower height	Obtained from optimization
		(SolarPILOT)
	Receiver diameter	Obtained from optimization
		(SolarPILOT)
	HTF type	Molten Salt (60 % NaNO ₃ + 40 %
		KNO ₃)
	Receiver flow pattern	Configuration 2
Heliostats Field	Layout configuration	Always optimize
	Heliostats length	12.2 m
	Heliostats width	12.2 m
	Water usage per wash	0.7 L/m^2
Atmospheric	Annual averaged AOD	0.3205
attenuation	Polynomial coefficient	-0.0037298
	0	
	Polynomial coefficient	0.154
	1	
	Polynomial coefficient	-0.0348
	2	
	Polynomial coefficient	0.0028768
	3	
Power Cycle	Condenser type	Air-cooled, wet-cooled and
		Hybrid
	Ambient temperature	31.6 $^{\circ}\text{C}$ for the air-cooled and
	at design	hybrid condensers
		14.3 °C for the wet-cooled
		condenser
Thermal Energy	Storage type	Two tanks
Storage	Tank height	20 m

Table 2Technical characteristics of the 10 MW wind turbines in SREP (adopted from Ref. [64]).

Parameter	Details
Turbine make and model	Siemens_Gamesa G97
Rated power per turbine (MW)	2
Number of turbines	5
Hub height (m)	78.98
Rotor diameter (m)	97
Swept area (m ²)	7390
Wind cut-in speed (m/s)	3
Wind rated speed (m/s)	11
Wind cut-off speed (m/s)	25
Distance between wind turbines (m)	330

inputs, such as the atmospheric attenuation polynomial function coefficients and condenser temperature at design, have been figured out specifically for the location of SREP. Table 1 shows the inputs of the SPT model which has been simulated in the SREP $(47.06^{\circ}\text{W}/29.20^{\circ}\text{S}/47.16^{\circ}\text{E}/29.30^{\circ}\text{N})$ where another 50 MW CSP (Parabolic Trough Collector), 10 MW WT and 10 MW PV plants are already in operation.

3.2.2. Wind turbines model

The WT used is Siemens-Gamesa G97 type, i.e. an identical type of the 10 MW pilot plant WT that is already in operation in SREP. The generated energy from this type of WT can be estimated from the turbine power curve that is provided by the manufacturer's catalogue [62] and this can be found in the supplementary materials. Based on the power curve, the following expression can provide the power of the simulated WT at any given hub height and wind speed [63]:

$$P_{WT}(t) = \begin{cases} \frac{v^k - v_C^k}{v_R^k - v_C^k} \cdot P_R v_C \le v \le v_R \\ P_R v_R \le v \le v_O \\ 0 \quad v \le v_C \quad \text{and} \quad v \ge v_O \end{cases}$$

$$(18)$$

where ν is the location's wind speed (m/s), ν_C is the cut-in wind speed, ν_O is the cut-out speed, ν_R is the rated wind speed, k is the Weibull shape factor and P_R is the rated power of the wind turbine.

3.2.2.1. Wind turbines validation. In a similar step to the SPT model validation, the WT here have been validated against the 10 MW wind farm in the SREP. The technical data of the operational 10 MW wind farm in SREP has been derived from Ref. [64] and are shown in Table 2 as follows:

Since the 5 WT of the 10 MW pilot plant are positioned in the north eastern part of the SREP rectangular shape, this work has simulated the first 5 WT in the exact same position as that in the pilot plant. Further, different numbers of WT have been simulated on the extension of the inclined upper border line of the SREP using the SAM's wind farm position import feature along with the approximate geometries of Fig. 5 (a). Other WT positioning and alignment scenarios have been simulated (see the supplementary materials), however, none of which has generated as good as the one implemented in reality in the SREP.

In addition, since the weather file is obtained from a freely available reanalysis model (PVGIS) in the form of a TMY, the wind speed is calculated at 10m of height. This hub height does not suit the simulation of the WT in this work as the WT in SREP are of 78m hub height. This can be resolved by interpolating the wind speed using the following correlation of the power law exponent as a function of the wind velocity and height [65]:

$$\alpha = \frac{0.37 - 0.088 \ln \left(U_{ref} \right)}{1 - 0.088 \ln \left(\frac{Z_{ref}}{10} \right)} \tag{19}$$

where U_{ref} is the mean wind speed at the reference height Z_{ref} . Thus, the wind speed at the desired height U_Z can be obtained as follows:

$$\frac{\mathbf{U}_{\mathbf{Z}}}{\mathbf{U}_{\mathbf{Z}_{ref}}} = \left(\frac{\mathbf{Z}}{\mathbf{Z}_{ref}}\right)^{\alpha} \tag{20}$$

3.2.3. SPT-WT hybridization

The integration of multiple renewable energy performance models in the SAM simulation tool is possible through the Generic Model feature. However, the Generic Model feature has only the ability to combine two or more already calculated performance models of several renewable energy technologies, while the automation of the combined models is not possible. This limits the ability of the SAM user in running any desired variation of one or more variable in one or both individual performance models in the combined configuration.

However, with the assistance of the provided LK automation tool, the user can perform mathematical operations on the individual separated performance models of different renewable technologies in the SAM in order to obtain the results of an integrated hybrid system. This can be achieved through the application of a parametric analysis which varies the design parameters of both technologies and then aggregate the outputs of each technology. This process can be done for the figures of interest, such as AEG, water consumption, CF and CAPEX.

3.3. Economics

The SAM financial model has got one of the most integrated and comprehensive economic tools and it uses different economic scenarios, e.g. Power Purchase Agreement (PPA), Single owner, partnership, etc. [66]. In this work, the single owner scenario is chosen as it fits the

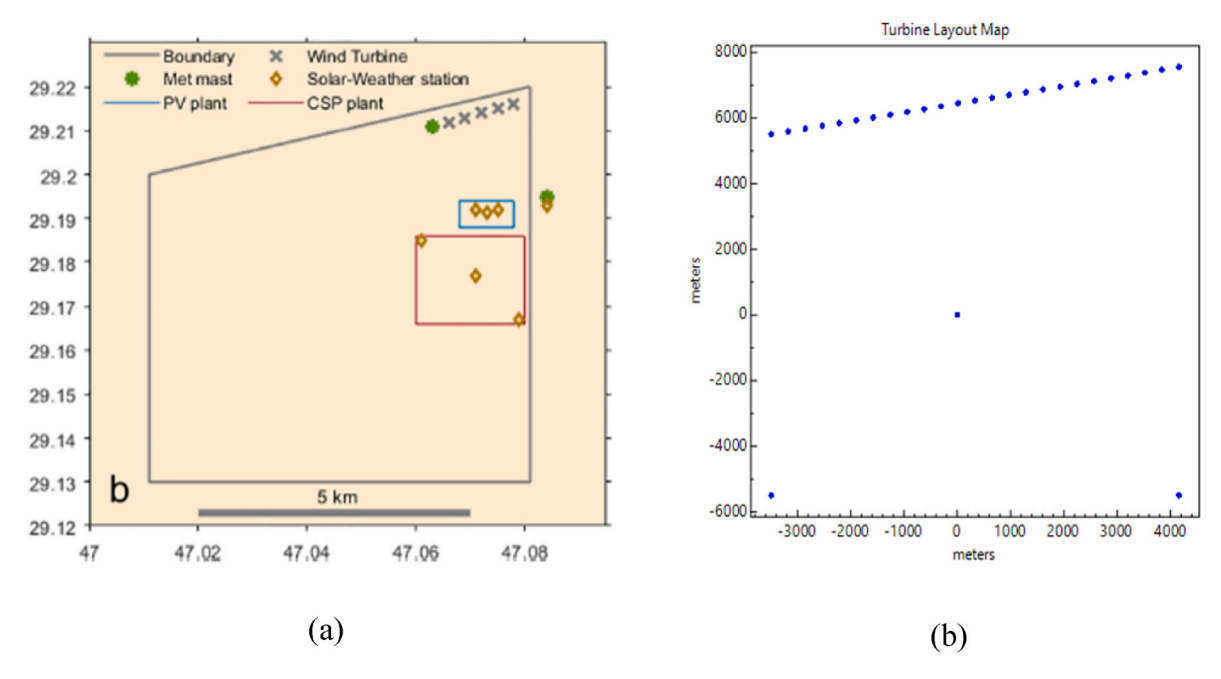


Fig. 5. (a) WT pilot plant in SREP [64] and (b) a total of 25 WT represented in the same location.

Table 3
LCOE calculation economic and design figures.

	Parameter	Details	description
SPT	Capacity	40-110 MW	_
		(gross)	
	AEG	Case dependent	Calculated and called fron
		•	SAM
	O&M fixed costs	66 \$/kW-y	NREL [73]
	O&M variable	3.5 \$/MWh	
	costs		
	PPA price	85 ¢/kWh	
	Total installed	Case dependent	Calculated and called from
	cost		SAM
	Net capital cost	Case dependent	
WT	Capacity	0-60 MW (net)	_
	AEG	Case dependent	Calculated and called from
			SAM
	O&M fixed costs	42 \$/kW-y	NREL [74]
	O&M variable	0 \$/MWh	E 13
	costs	,	
	PPA price	4 ¢/kWh	
	Total installed	Case dependent	Calculated and called from
	cost		SAM
	Net capital cost	Case dependent	
Hybrid	Inflation rate	2.4 %/year	For Kuwait [75]
plant	Real discount	3.5 %/year	For Kuwait [76]
	rate	,,,	
	Nominal	5.98 %/year	Calculated and called from
	discount rate		SAM
	Annual interest	4 %	For Kuwait [77]
	rate		
	Federal tax	17 %	Kuwait Corporate, Zakat
			and KFAS tax [71]
	State tax	0 %	_
	Term tenor	18 years	Default values in SAM
	Debt size	50 % of total	
		installed cost	
	Debt upfront fee	450000 \$	
	Debt closing fee	2.75 % Of debt	
	Interest on	1.75 %/year	
	reserves		
	Insurance rate	0.5 % of total	
		installed cost	

Table 4The WT validation against the reported data in Ref. [64].

	Present work	Reported data for the 1st year	Reported data for the 2 nd year	Contractor guarantee
AEG (GW/y)	34.1	39.6	36.9	35.2
Capacity Factor (%)	38.9	45.2	42.1	_

country's policy for government renewable energy shift under the 2030 vision of new Kuwait [67].

3.3.1. Hybrid SPT-WT configurations' economics

The SAM software, along with the nested LK scripting language, have been used to automate the calculation of the LCOE for any integrated SPT-WT system while varying the design variables in the performance models of the hybrid configuration. Both SPT and WT models have been simulated individually, and the LK has been used in order to break down the LCOE cash flow sheets of both individual models. Then all the essential economic figures that contributes in the calculation of the LCOE in each individual performance model has been added up in order to calculate a LCOE for all the SPT-WT hybrid configuration. The following equations (20)–(34) are adopted from the SAM cash flow data sheets [68] for the LCOE calculations as follows:

$$LCOE = \frac{-C_0 - \frac{\sum_{n=1}^{N} C_n}{(1 + d_{noninal})^n}}{\frac{\sum_{n=1}^{N} Q_n}{(1 + d_{non})^n}}$$
(21)

where Q_n is the Net Present Value (NPV) of the AEG over the entire analysis period N, C_0 is the project equity, C_n is the NPV of the annual costs of the project, d_{real} is the discount rate, $d_{nominal}$ is the nominal discount rate and n is the analysis year [69]. The NPV of the AEG is calculated as follows:

$$Q_{n=} \frac{AEG_n}{\left(1 + d_{real}\right)^n} \tag{22}$$

The AEG of the hybrid plant is the sum of both technologies energy generation:

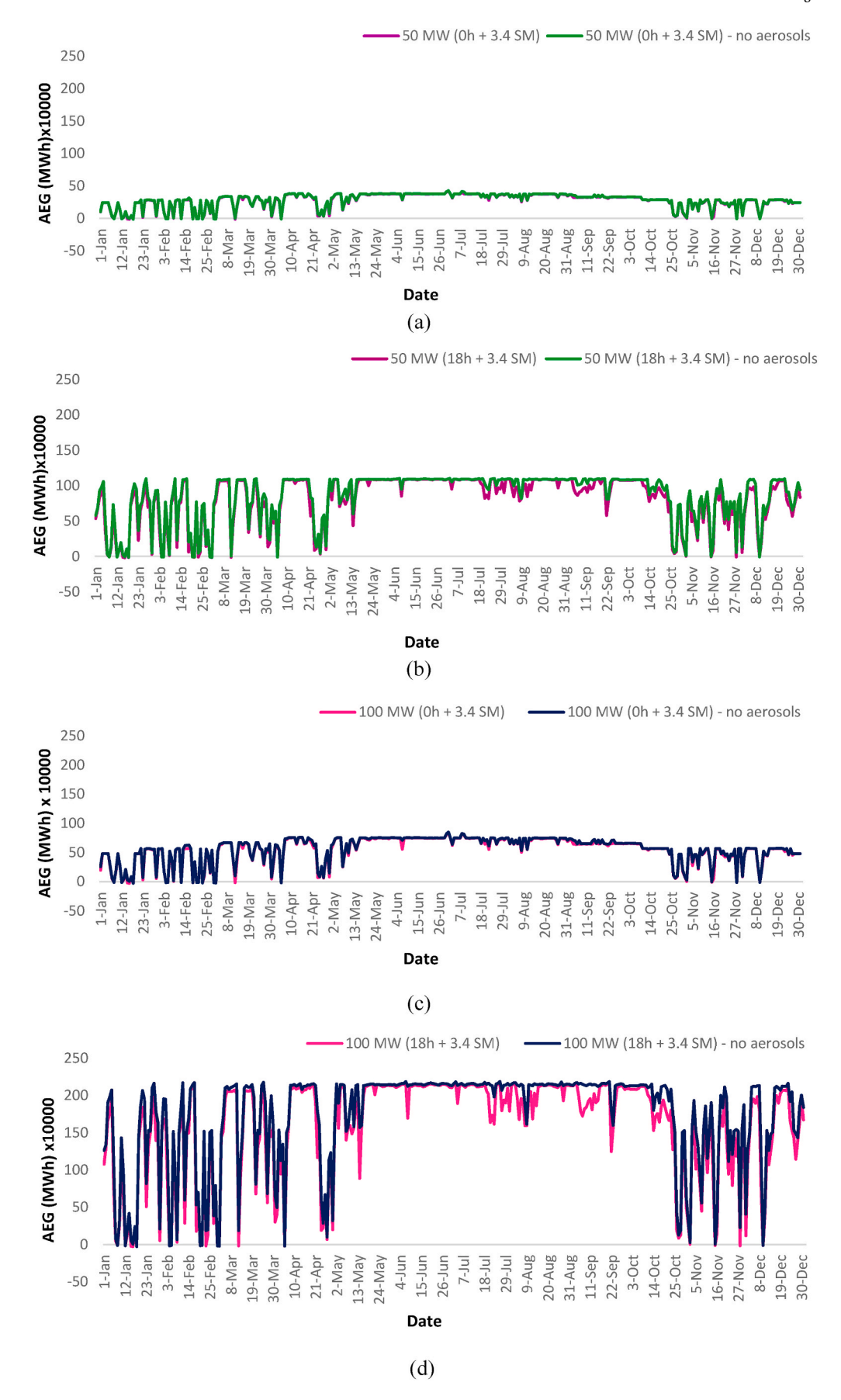


Fig. 6. Aerosols inclusion effect on the standalone SPT for (a) 50 MW with 0 h TES, (b) 50 MW with 18 h TES, (c) 100 MW with 0 h TES and (d) 100 MW with 18 h TES.

M.S. Alfailakawi et al. Results in Engineering 24 (2024) 102968

Table 5
The 50 and 100 MW standalone SPT optimal TES-SM outputs based on the annually averaged AOD and compared to the no aerosols scenario.

50 MW									
TES	Optimal SM	Thermal power from	SF (MW _{th})	Total absorbed energy	y (MW _{th})	AEG (GW)		LCOE (¢/kWh)	
(h)	(-)	Annually averaged AOD	No aerosols	Annually averaged AOD	No aerosols	Annually averaged AOD	No aerosols	Annually averaged AOD	No aerosols
0	1.4	291.7	297.6	273.8	279.4	91.8	94	19.2	18.6
3	1.8	400.8	434.9	378.7	412.4	134.9	138.1	15.6	15.2
6	2.2	507.8	563.9	479.2	534.7	175.4	180.2	14.1	13.6
9	2.6	606.1	680.4	574.7	648.2	212.1	219.4	13.2	12.8
12	2.6	660.3	734.4	628.6	702.1	227.9	243.3	12.7	11.9
15	3	763.7	860.1	725.1	820.7	265.8	284.1	12.3	11.5
18	3.4	843.7	963.2	799	917.3	300	317.8	12.1	11.4
100 MV	V								<u>-</u>
TES	Optimal SM	Thermal power from	SF (MW _{th})	Total absorbed energy	y (MW _{th})	AEG (GW)		LCOE (¢/kWh)	
(h)	(-)	Annually averaged	No	Annually averaged	No	Annually averaged	No	Annually averaged	No
		AOD	aerosols	AOD	aerosols	AOD	aerosols	AOD	aerosols
0	1	507.6	531.7	482.4	506.3	157.1	166.5	18.6	17.6
3	1.4	717.8	793.8	683.9	759.1	236.6	254.2	15.3	14.3
6	1.8	922.3	103,8.9	878	993.5	311.2	335.5	14	13
9	2.2	1116.3	1272.6	1063.1	1217.8	380.8	411.6	13.3	12.3
12	2.6	1324.3	1534.7	1254.7	1462.9	456.9	494	12.7	11.8
15	3	1517	1778.7	1438.8	1697.9	527.6	570.5	12.4	11.5
18	3.4	1659.5	1979.2	1573.7	1890.3	574.2	630.2	18.1	16.6

$$AEG_n = AEG_{SPT_n} + AEG_{WT_n} \tag{23}$$

In a similar manner, the NPV of the annual costs is calculated as follows [70]:

$$C_{\rm n} = \frac{Annual\ Costs_n}{\left(1 + d_{nominal}\right)^n} \tag{24}$$

While the AEG is simply both the SPT and the WT energy generation on annual scale, the plant annual costs involves all the considered economic parameters of both technologies and is calculated as follows [68]:

Annual $Costs_n = federal tax benefit_n + state tax benefit_n - total expenses_n$

- working capital reserve funding,
- working capital reserve realease of funds_n
- debt service reserve funding_n debt service reserve release of funds_n
- debt interest payement_n debt principal payement_n
- + interest on reserve_n

(25)

Since Kuwait is a state with multiple governorates (which are not subject to taxation), the total tax rate in the SAM has been assigned a value of 17 %, i.e. an aggregation of the corporate tax of Kuwait (15 %), both Islamic compulsory charity (Zakat 1 %) and the Kuwait Foundation for the Advancement of Sciences (KFAS) support (1 %) [71]. The total tax benefit and income are calculated as follows:

total tax benefit_n = total taxable income_n*tax rate
$$_{corporate+Zakat+KFAS}$$
 (26)

This makes the federal and state taxable incomes available as follows [68]:

total taxable income_n = $EBITDA_n$ + interest on reserve_n

$$-$$
 debt interest payement_n (27)

where EBITDA is the Earnings before Interest, Taxes, Depreciation and Amortization and is calculated as follows [72]:

$$EBITDA_n = total\ revenue_n - total\ expenses_n$$
 (28)

As for the interest on the reserve and the debt interest payment, these are calculated as follows:

interest on
$$reserve_{n+1} = total reserve_n * reserve interest$$
 (29)

debt interest $payement_n = debt$ ending $balance_{n-1} - term$ interest $rate_n$

(30)

The total expenses include all the spending of the plant and these are calculated as follows [68]:

 $total\ expenses_n = insurance_n + electricity\ purchase_n$

- + O&M production based expenses_n
- + O&M production capacity expenses_n (31)

where the electricity purchase is the cost of the electricity that the plant purchases from the grid when it is required. Since the WT does not require any electricity from the grid, the electricity purchase is a unique function of the amount of electricity required for the SPT based on an agreed Power Purchase price (PPA). The same PPA can be used for specifying the price of selling the power unit, which makes the total revenue a function of the AEG and the PPA as follows:

$$total\ revenue_n = AEG_{SPT+WT} * PPA_{SPT+WT}$$
(32)

It is worth mentioning that despite the reasonable amount of information that exists in the literature about the PPA of renewable energy technologies, such as SPT and WT, there is a lack of such price details for a combined system. Thus, the PPA in this work has been calculated based on both the SPT and WT PPA prices from the NREL in addition to each technology's individual capacity share from the overall hybrid plant capacity as follows:

$$PPA_{SPT+WT} = PPA_{SPT} * \frac{Capacity_{SPT}}{Capacity_{SPT+WT}} + PPA_{WT} * \frac{Capacity_{WT}}{Capacity_{SPT+WT}}$$
(33)

Also, the O&M capacity based expenses of the hybrid plant, which is a part of the total expenses, is calculated in a quite similar manner as follows:

O&M capacity_{SPT+WT} = Fixed
$$Costs_{SPT}^*$$
 $\frac{Capacity_{SPT}}{Capacity_{SPT+WT}}$
+ Fixed $Costs_{WT}^*$ $\frac{Capacity_{WT}}{Capacity_{SPT+WT}}$ (34)

The O&M production based expenses is uniquely a factor of the SPT variable expenses as the variable costs of the WT is equal to zero:

$$O\&M\ production_{SPT+WT} = Variable\ Costs_{SPT} *AEG_{SPT}$$
(35)

M.S. Alfailakawi et al. Results in Engineering 24 (2024) 102968

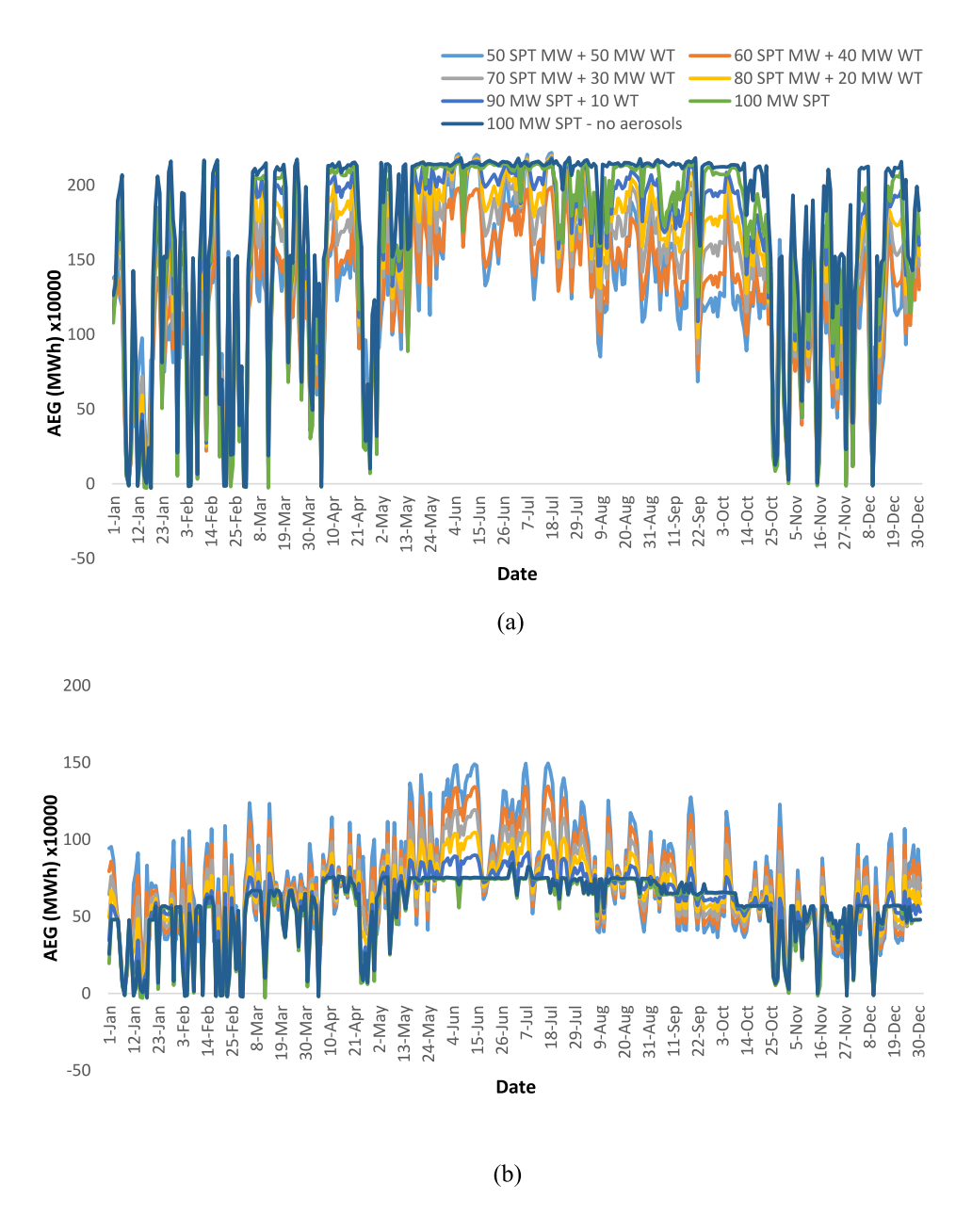


Fig. 7. The performance of a 100 MW hybrid SPT-WT model with different shares of both technologies compared to the 100 MW standalone SPT with and without considered aerosols for (a) 18h of TES and (b) 0h of TES.

The lifetime of the project is 25 years, and the main economic assumptions and parameters are shown in Table 3.

4. Results & discussion

4.1. SPT & WT models validation

The validation of the SPT base model for this work has been originally carried out in a previous work by the authors [27] (see for details the supplementary materials). The validation is based on two steps in which the SPT base model has been validated against both commercial scale and simulated data from the literature. In addition, the WT modelling results have been compared with pilot plant data (over two years) from SREP that is available in Ref. [64]. As depicted in Table 4 the modelling results are in good agreement with the pilot data:

The deviation of this work's results compared to the first year of

operation of the WT plant is found to be equal to $-13.9\,\%$. This improves in the second year to $-7.59\,\%$. Interestingly, the contractor company had assured a $35.2\,\mathrm{GW/y}$, which is only $-3.13\,\%$ from the modelled AEG in this work. The differences can be attributed to the weather file that we have used. This is a TMY file that describes the metrological conditions over an extended period of time, and it is expected to give more accurate results when compared to the long-term operational data.

4.2. Aerosols impacted SPT performance

Regarding the assessment of the aerosols effect, it is critical to select a specific point to assess the solar field performance as both the TES-SM are expected to majorly contribute in the definition of the aerosols effect on the AEG. Thus, for simplicity, the TES and SM configurations with the probable best techno-economic outputs (18h and 3.4 of SM) has been chosen as reference point at which the AEG is observed. In addition, the

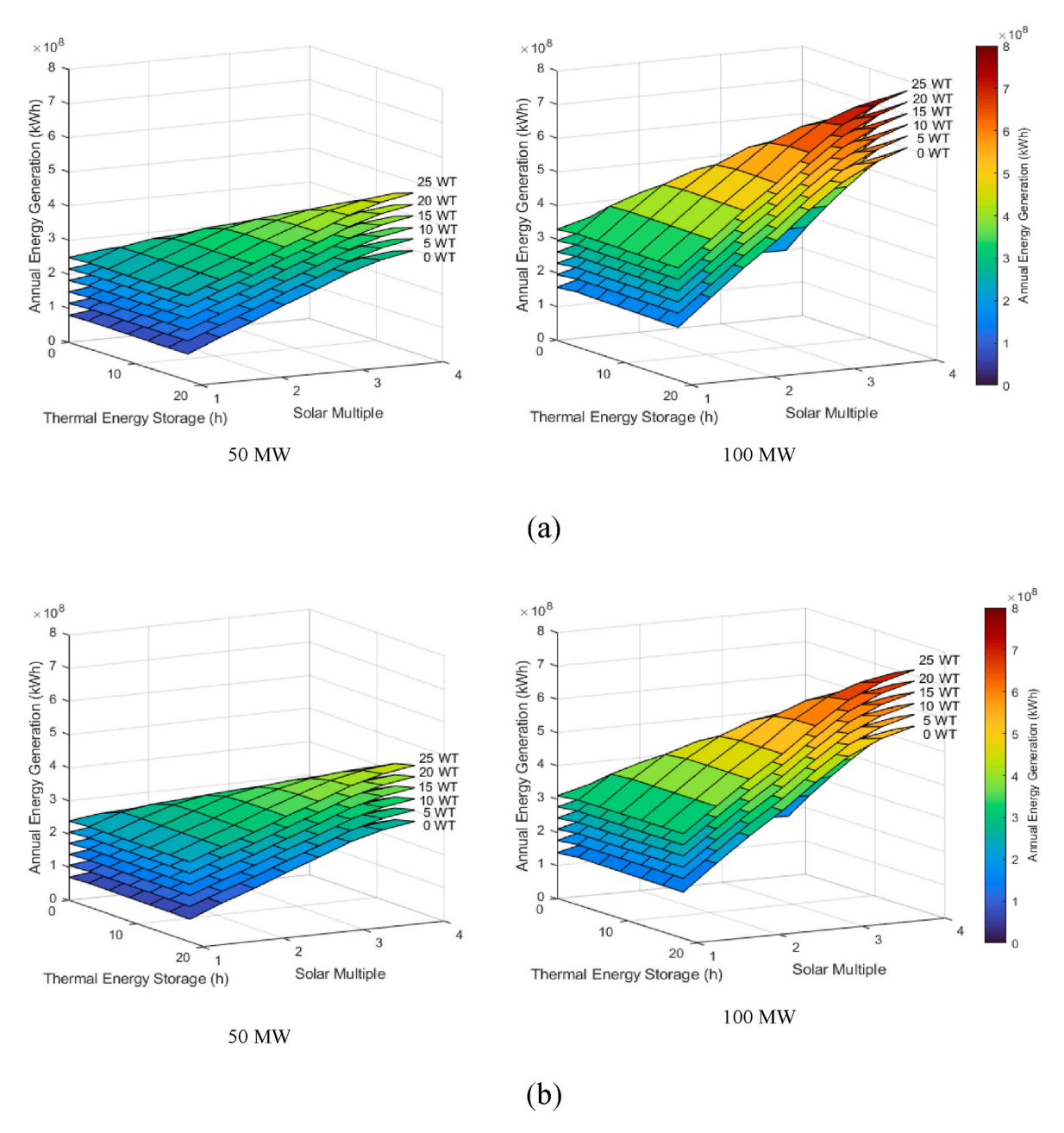


Fig. 8. The variation of the annual energy generation for different SPT + WT capacities based on 4 scenarios: (a) water-cooled condenser, (b) air-cooled scenario, (c) 30 % hybrid and (d) 19 % hybrid scenario.

configuration with the same SM value but with no TES inclusion is examined in Fig. 6, which illustrates the assessment of both SPT 50 MW and 100 MW capacities.

An increase in the TES capacity results in an increase in the AEG. However, as it can be seen in Fig. 6, the effect of aerosols on the TES scenario is greater than without TES. This is due to the fact that in the case where there is no TES included, a limited amount of thermal energy is reflected on the receiver and thus attenuated by the aerosols. The limitation is set by the small SM of the solar field which is only enough to run the power cycle at its rated capacity without any excess. On the other hand, in the case where a TES is included, a large value of SM is required to fully exploit the TES, hence more thermal energy from the solar field is used, thus more attenuation is found.

Since the SM represents the solar field size relative to the plant capacity, a similar value of SM does not represent the same solar field size,

thus the solar field sizes in Fig. 6 are not of the same size. For instance, the solar field of the 100 MW standalone SPT is larger than that of the 50 MW standalone SPT despite having a similar value of SM (here 3.4). In addition, regarding the reflectors shading effect, the reflectors, in the case of the SM is to increase, are added at the outer circumference of the existing ones. As a result, larger slant ranges from larger solar fields are produced which theoretically should amplify the effect of the aerosols on the reflected irradiance. The latter is indeed what is found in this work, however, not with a sharp amplitude. For example, the difference found between the AEG of the 50 MW SPT that is impacted by aerosols and that of the no aerosols SPT of the same capacity (and the same 18h TES and 3.4 SM) is found to be 5.8 % and the difference in the AEG of the same cases but for the 100 MW SPT is found in this work to be 9.1 %.

As depicted in Table 5, the deviations in the AEG due to aerosols inclusion result in deviations in the LCOE. The deviation in the AEG is

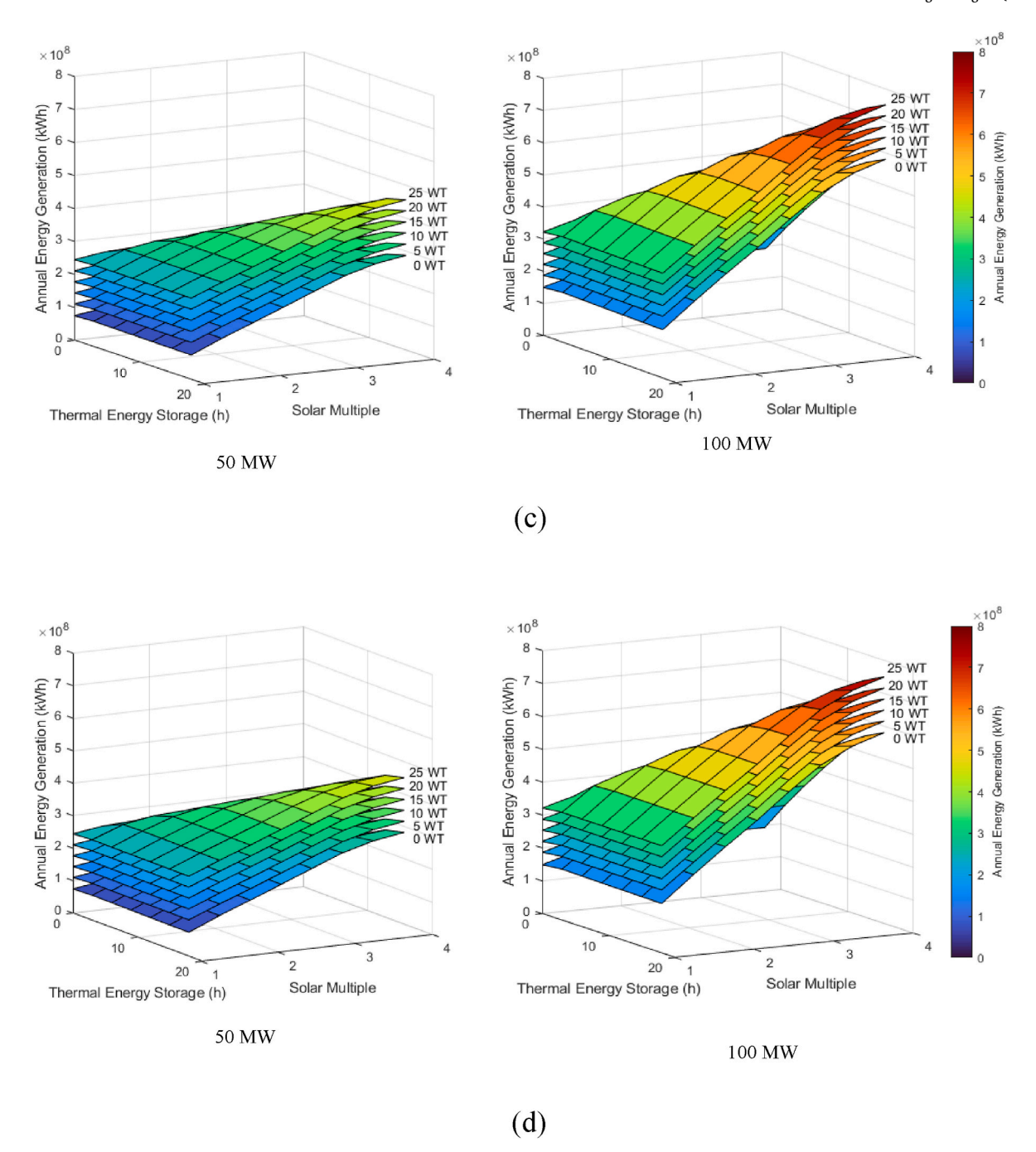


Fig. 8. (continued).

 Table 6

 Performance comparison of the different condenser types for 50–100 MW SPT. The water-cooled condenser is used as reference point for comparisons.

	Condenser 7	Condenser Type						
	Wet-Cooled		Air-Cooled		30 % Hybrid		19 % Hybrid	
	50 MW	100 MW	50 MW	100 MW	50 MW	100 MW	50 MW	100 MW
Annual Energy	3E+08	5.89E+08	2.77E+08	5.41E+08	2.92E+08	5.73E+08	2.9E+08	5.7E+08
Generation (kWh)								
Deviation (%)	N/A	N/A	-7.7	-8.2	-2.7	-2.7	-3.3	-3.2
Water Consumption (m ³ /y)	973449	1956066	68216.6	143407	440821	889138	305507	617549
Deviation (%)	N/A	N/A	-93	-92.7	-54.7	-54.5	-68.6	-68.4
Levelized Cost of Energy (¢/kWh)	12.1	12.3	13.2	13.5	12.6	12.8	12.6	12.9
Deviation (%)	N/A	N/A	8.3	8.8	4.4	4.3	4.4	5.2
Capacity Factor (%)	68.5	67.3	63.2	61.8	66.6	65.4	66.3	65.1
Deviation (%)	N/A	N/A	7.7	8.2	2.8	2.8	3.2	3.3

Table 7The upper and lower limits of the variables based on the assigned step sizes.

Parameter	Lower bound	Upper bound	Step size
SPT _{capacity}	50	100	10
SM	1	3.8	0.4
TES	0	18	3
WT_n	0	25	5

first captured in the form of less reflected thermal energy from the solar field to the receiver. As a consequence, less thermal energy is transferred from the receiver to the HTF and thus, less thermal to electrical energy conversion. This is project at the LCOE as the latter is deviated as a result of the AEG deviation. For the 50 MW capacity, the LCOE of the no aerosols scenario is found to be 5.9 % less than that of the annually

averaged AOD scenario. As for the 100 MW capacity, the LCOE of the no aerosols scenario is found to be 9 % less than that of the annually averaged AOD scenario (both at 18h of TES and 3.4 SM).

4.3. Aerosols impacted SPT and WT hybridization

In this section, different SPT-WT configurations are examined under the condition that the hybrid configuration is always 100 MW. All observed SPT-WT configurations are compared to a theoretical optimally performing plant which is represented by the no-aerosols 100 MW standalone SPT at the same TES-SM configuration, as this is expected to generate the highest AEG among all other configurations of SPT and/or SPT-WT as illustrated in Fig. 7.

Despite the inclusion of the aerosols effect on the solar field, the

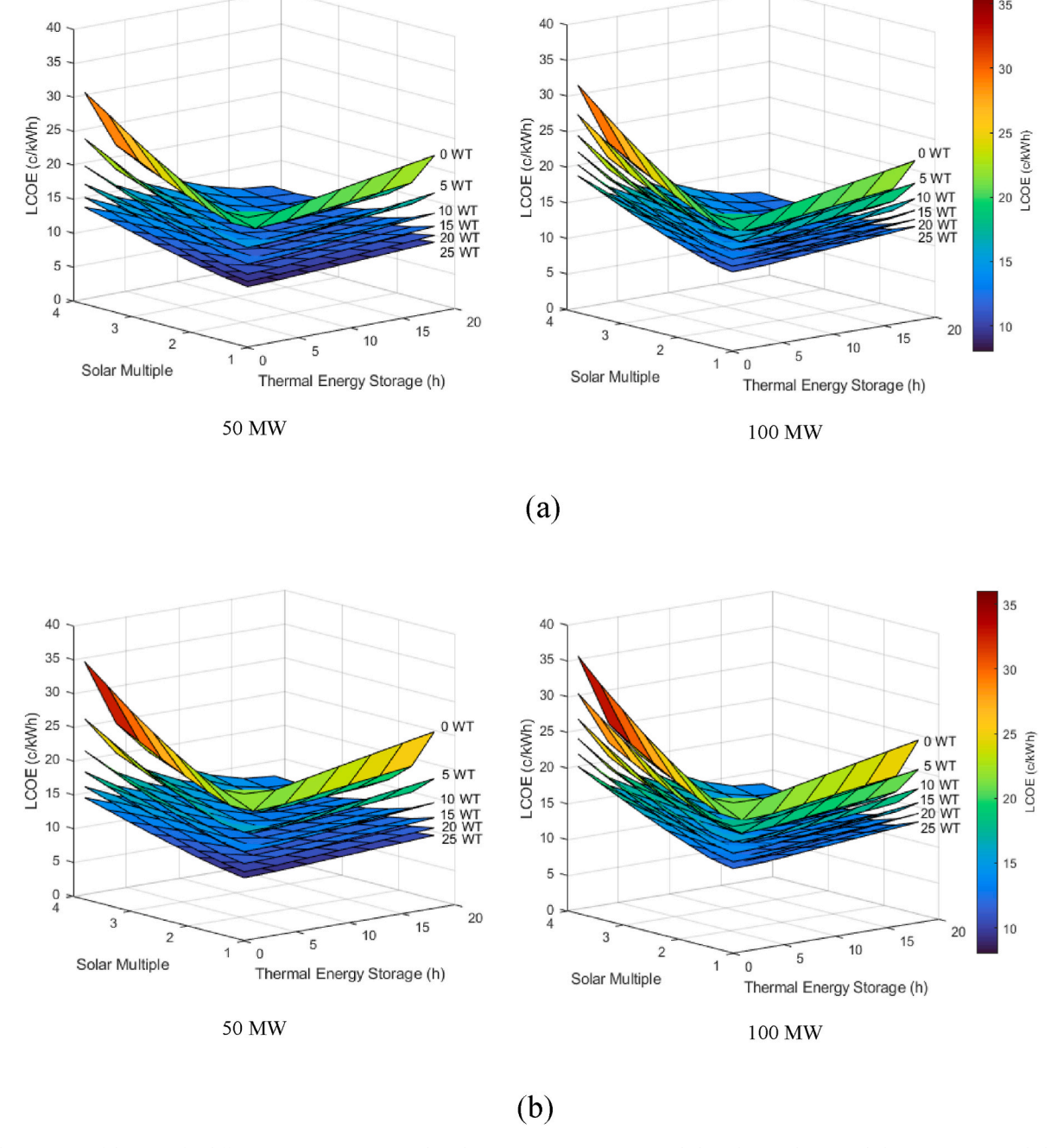


Fig. 9. The variation of the LCOE for different SPT + WT capacities based on 4 scenarios: (a) water-cooled condenser, (b) air-cooled scenario, (c) 30 % hybrid and (d) 19 % hybrid scenarios.

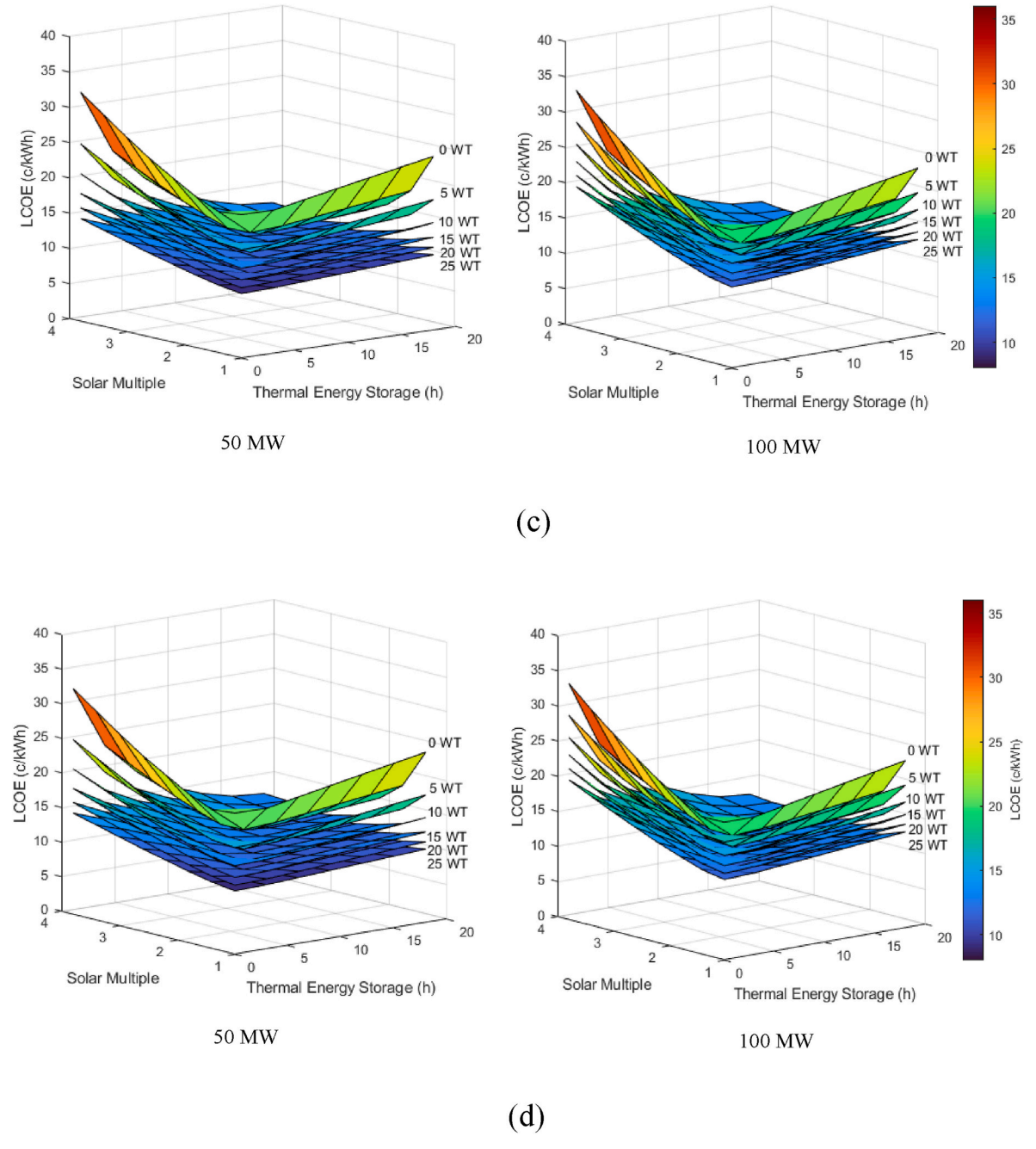


Fig. 9. (continued).

standalone aerosols impacted 100 MW SPT outperforms all other SPT-WT configurations as the WT integration fails to fully compensate the loss of the AEG caused by the aerosols density. The configurations with a major share of WT outperforms those of major shares of SPT only for few days over the entire year, e.g. first and mid-July. This is mainly due to the lack of energy storage for the WT. The latter finding is also obvious in the AEG of the configurations with a major SPT share as these assure an almost steady energy supply over the entire summer season. Interestingly, in the case of TES exclusion, which is illustrated in Fig. 7 (b), the configurations with the major share of WT outperform those of smaller WT share. This agrees with previous studies findings that the intensity of the wind resource of this case study location has a great potential. Also, only from AEG prospective, this proves that the SPT is way less valuable without a TES deployment as the large solar field is dumbing all the excessive thermal energy.

Beyond the AEG, the SPT-WT is affected by the variation of each technology's share as the WT integration drives the LCOE and the water consumption down, while the TES inclusion with the bigger SM values, on the other hand, drives the AEG and CF up. This contradiction resulting from these assigned conflictive objectives is solved through a multi-objective optimization, as this technique is able to present a set of optimal solutions which represent a trade-off between the objective functions.

4.4. SPT different condenser cooling scenarios

Table 6 summarises the results for the four different condenser cooling scenarios. The comparison excludes the WT as the former does not consume any water and for the sake of simplification, a certain TES-SM configuration is presented, i.e. 18h of TES and a 3.4 SM. The results

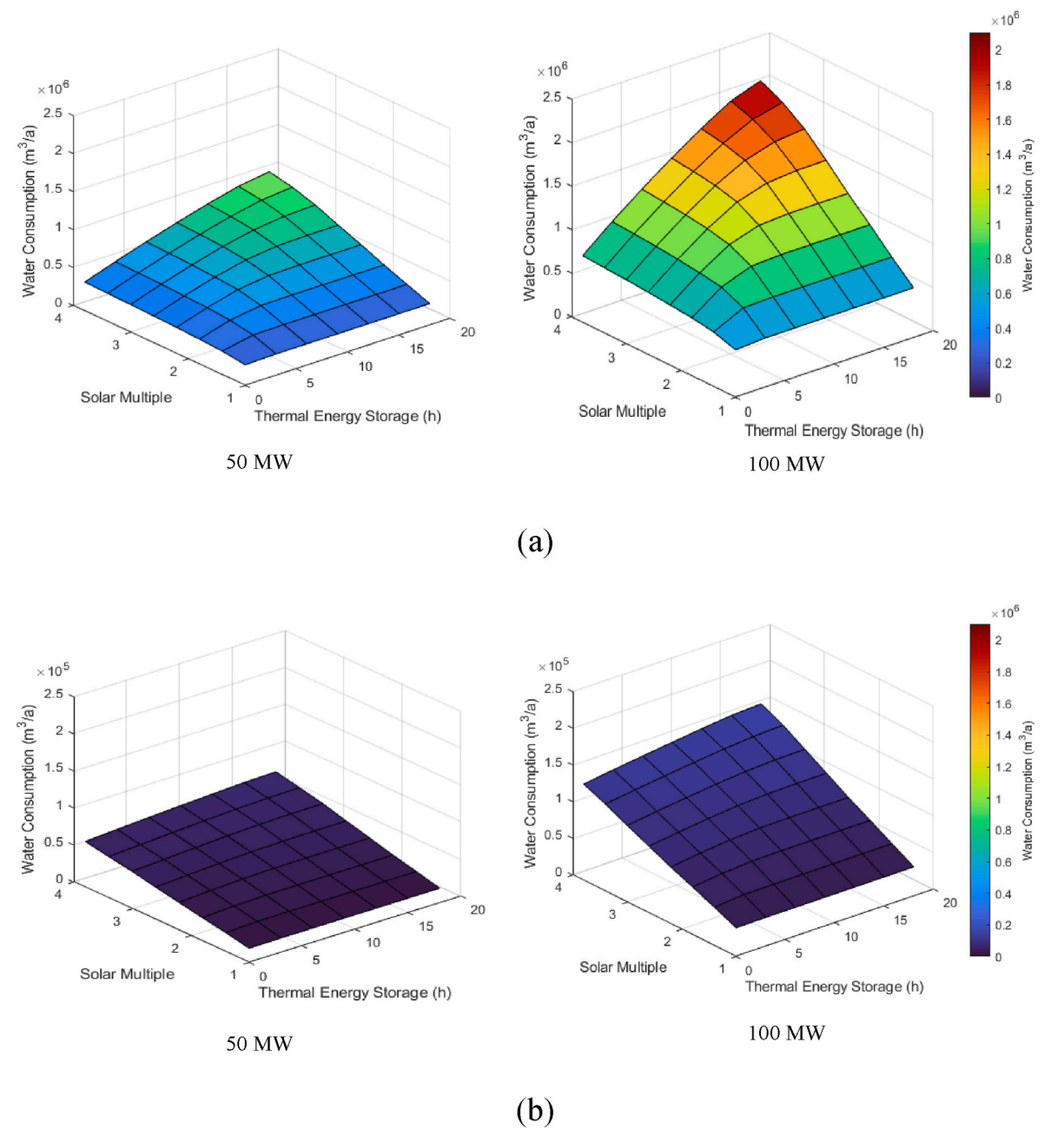


Fig. 10. The variation of the annual water consumption for different SPT + WT capacities based on 4 scenarios: (a) water-cooled condenser, (b) air-cooled scenario, (c) 30 % hybrid and (d) 19 % hybrid scenarios.

tabled in Table 6 confirms that the AEG of the water-cooled condenser scenario excels and outperforms all other scenarios as a result of the better heat rejection of the water at the power cycle. This is projected at the CF as the latter of the water-cooled scenario is the highest, however, the water consumption is the highest too. Both LCOE values of the 50 and the 100 MW water-cooled scenario are the lowest compared to the other scenarios. The scenario with the second highest AEG and CF is the 30 % hybrid condenser and this is followed by the 19 % scenario, while the air-cooled scenario is found to be the lowest in these terms due to the partial role of water cooling for the 30 % and 19 % compared to the dry cooling of the air-cooled condenser. In contrast, the air-cooled condenser saves up to 93 % of the used water compared to the water-cooled one and this indicates that the mirrors washing only consumes 7 % on the consumed water. Both hybrid scenarios present intermediate

water consumption rates as for instance, the 30 % hybrid scenario consumes 54.5 % less water for only 2.7 % less AEG compared to the water-cooled condenser scenario of the 100 MW SPT. Similarly, the 19 % hybrid scenario generates 3.2 % less AEG, however for a 68.4 % less consumed water.

4.5. SPT - WT hybridization

This section is carried out in order to understand the effect of the variation of each variable on the important metrics of the hybrid SPT-WT model. Variables such as WT_n and TES-SM are varied over different ranges just to observe how the AEG, CF, water consumption and LCOE behave. For the sake of simplicity, only two different capacities of SPT have been taken in consideration for this step: a small

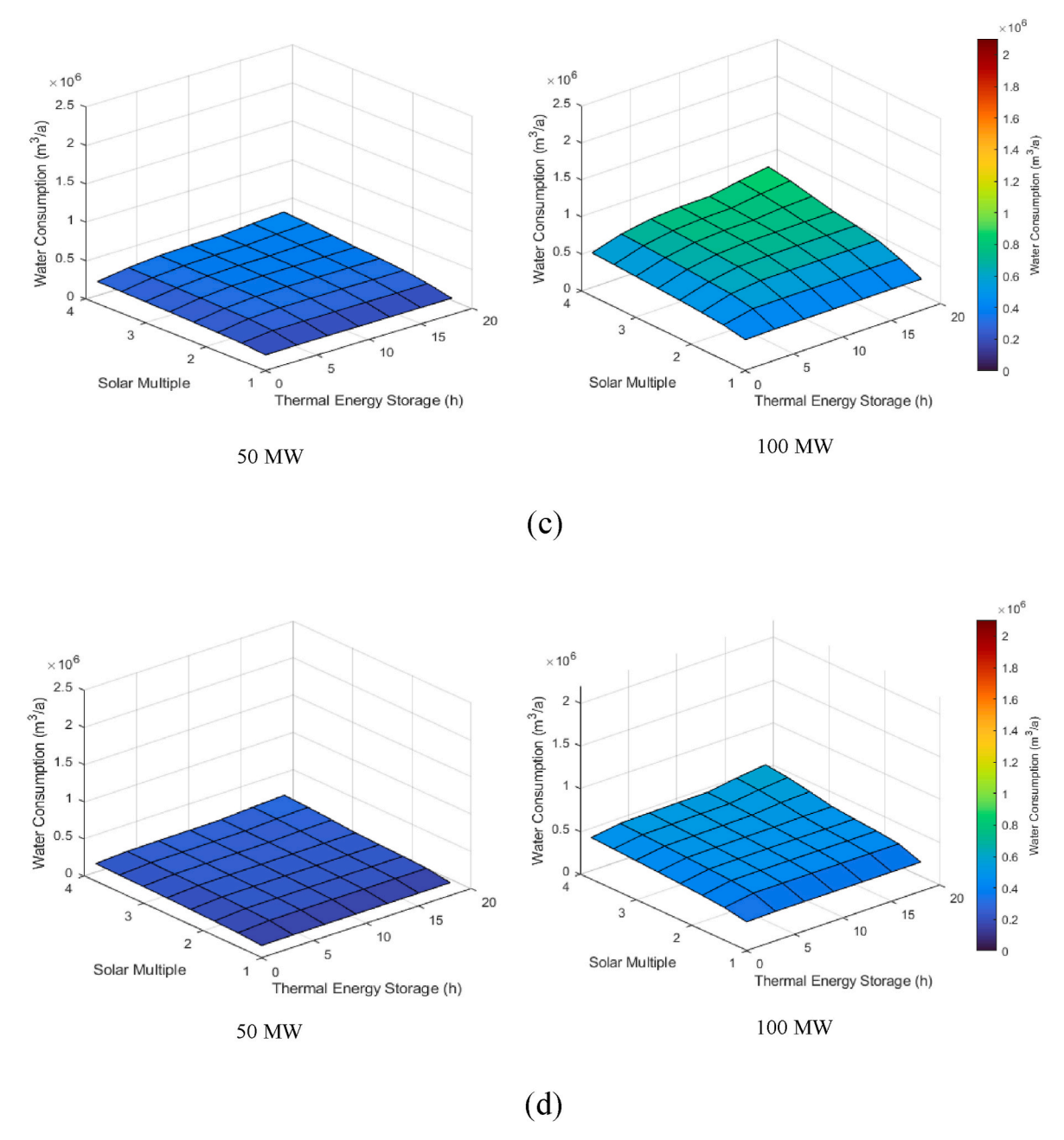


Fig. 10. (continued).

capacity of 50 MW and a large one of 100 MW while the rest of the variables follow the step sizes indicated in Table 7.

Fig. 8 illustrates the effects of the variation of the designated variables on the AEG where (a) is the AEG of the water-cooled condenser scenario, (b) is for the air-cooled scenario, (c) is for the 30 % hybrid scenario and (d) is for the 19 % hybrid scenario. Logically, the increase in the TES-SM as well as in the SPT capacity results in an increase of the AEG. Similarly, the increase in the WT number yields in an obvious proportional increase of the AEG. This is because an increased SM stands for a bigger solar field size, thus more collected thermal energy from the solar field. In addition, the larger the TES capacity the bigger is the ability to store the excessive energy from the solar field for later usage. The bigger SPT capacity implies both a bigger solar field and a bigger thermal to electrical energy conversion as a result of a bigger power cycle. Lastly, because of the absence of a storage system for the WT, the increase in latter's capacity is linear as each added WT adds a similar amount of AEG to the total AEG of the hybrid configuration. As for the

condenser cooling types, a minor superiority has been observed in the water-cooled condenser scenario over the other scenarios of air and hybrid cooling.

Also, the integration of WT with the SPT yields positive economic returns as the bigger WT capacity integrated in the hybrid configuration, the lower the LCOE becomes. This is because of the lower CAPEX of the WT when compared to that of the SPT. Fig. 9 shows the effect of the variation of the decision variables on the LCOE where it has been noticed that the greatest decrease of the LCOE is a result of the addition of the largest WT number. Further, it can be observed that the rate of decrease in the LCOE becomes smaller as the number of the WT is increasing. This trend is most probably due to the lack of a sufficient additional amount of WT energy that could further reduce the LCOE. More energy could be generated by employing a WT back-up system, but this is associated with high expenses.

As for the effect of the cooling type on the LCOE, it is noticed that the air-cooled scenario yields slightly higher LCOE values compared to all

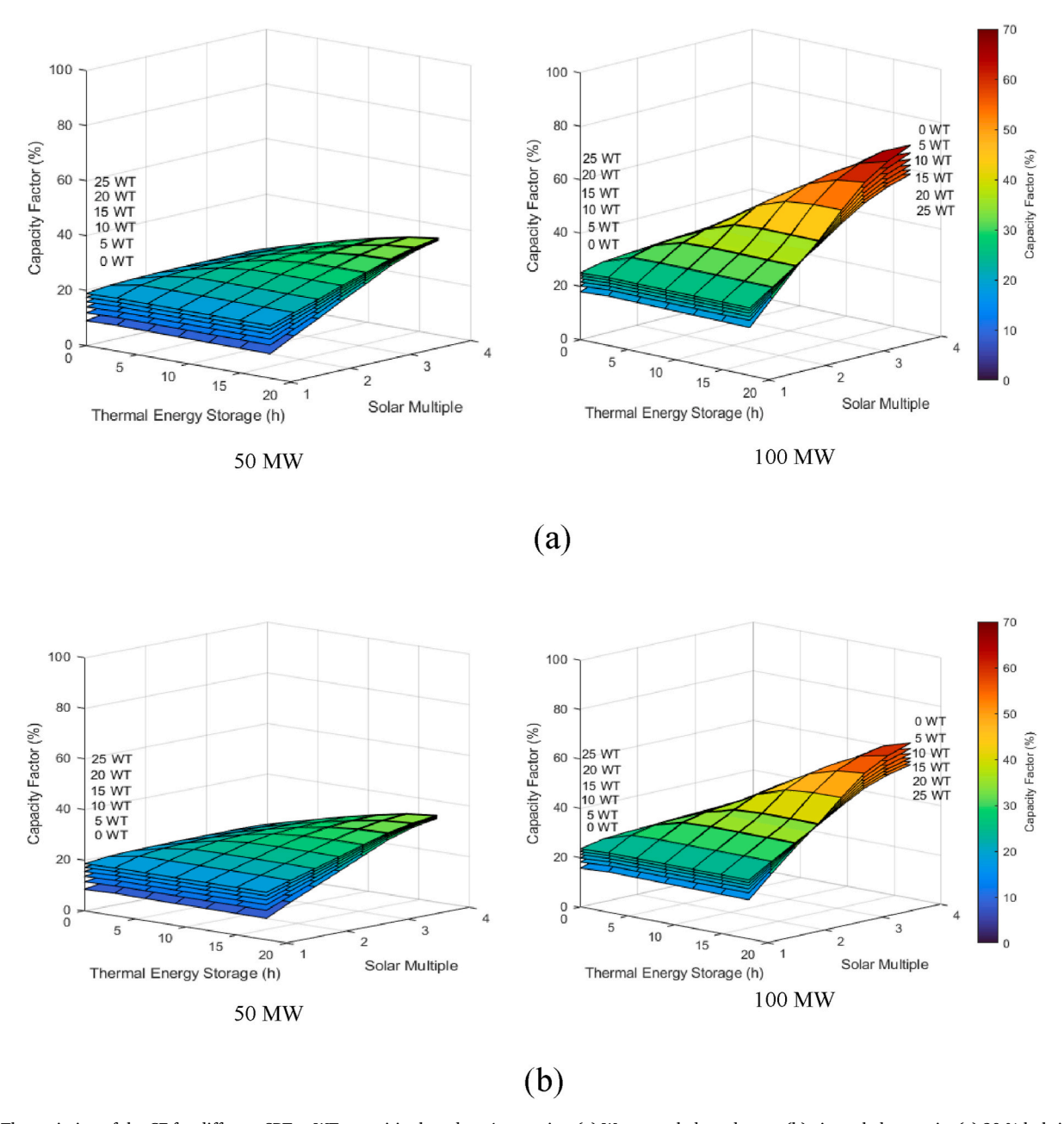


Fig. 11. The variation of the CF for different SPT + WT capacities based on 4 scenarios: (a) Water-cooled condenser, (b) air-cooled scenario, (c) 30 % hybrid and (d) 19 % hybrid scenarios.

other condenser cooling scenarios. This is more obvious on the standalone SPT configuration prior to any WT integration and most probably due to two reasons, i.e. lower thermal to electrical conversion rates at the power cycle due to less efficient heat rejection process by air and the second reason due to the higher CAPEX of the air-cooled condenser compared to the water-cooled one.

Regarding the water consumption, the water-cooled condenser scenario consumes relatively huge amounts of water compared to all the other condensers. Fig. 10 illustrates the variation in the water consumption among the four adopted scenarios in which the air-cooled scenario consumes drastically less water. This amount of water in the air-cooled scenario is dedicated to the washing of the solar field reflectors and this can be seen in Fig. 10 (b) where the large increase in the water consumption is paired with the increase of the SM.

The advantages due to the WT integration are, on the other hand, met with some expected limitations on some important performance indicators such as the CF. The importance of such an indicator relies in the fact that this work is not following any load demand, but instead, a specific rated capacity is targeted to be fulfilled for each SPT-WT configuration. In this work, it has been found that the bigger the added WT capacity to the hybrid configurations, the lower the CF becomes, as shown in Fig. 11. That is because the added AEG from the WT is not enough to increase the CF as illustrated in Equation (35). Interestingly, for the 100 MW SPT capacity, when the SM and TES capacity increase the addition of WT gradually reduces the CF; and eventually the scenario with no WT even if at low SM and TES values exhibits the lowest CF, at the peak of these parameters (SM and TES) features the highest CF compared to all scenarios with WT. The opposite trend is observed for the scenario that employs 25 WT.

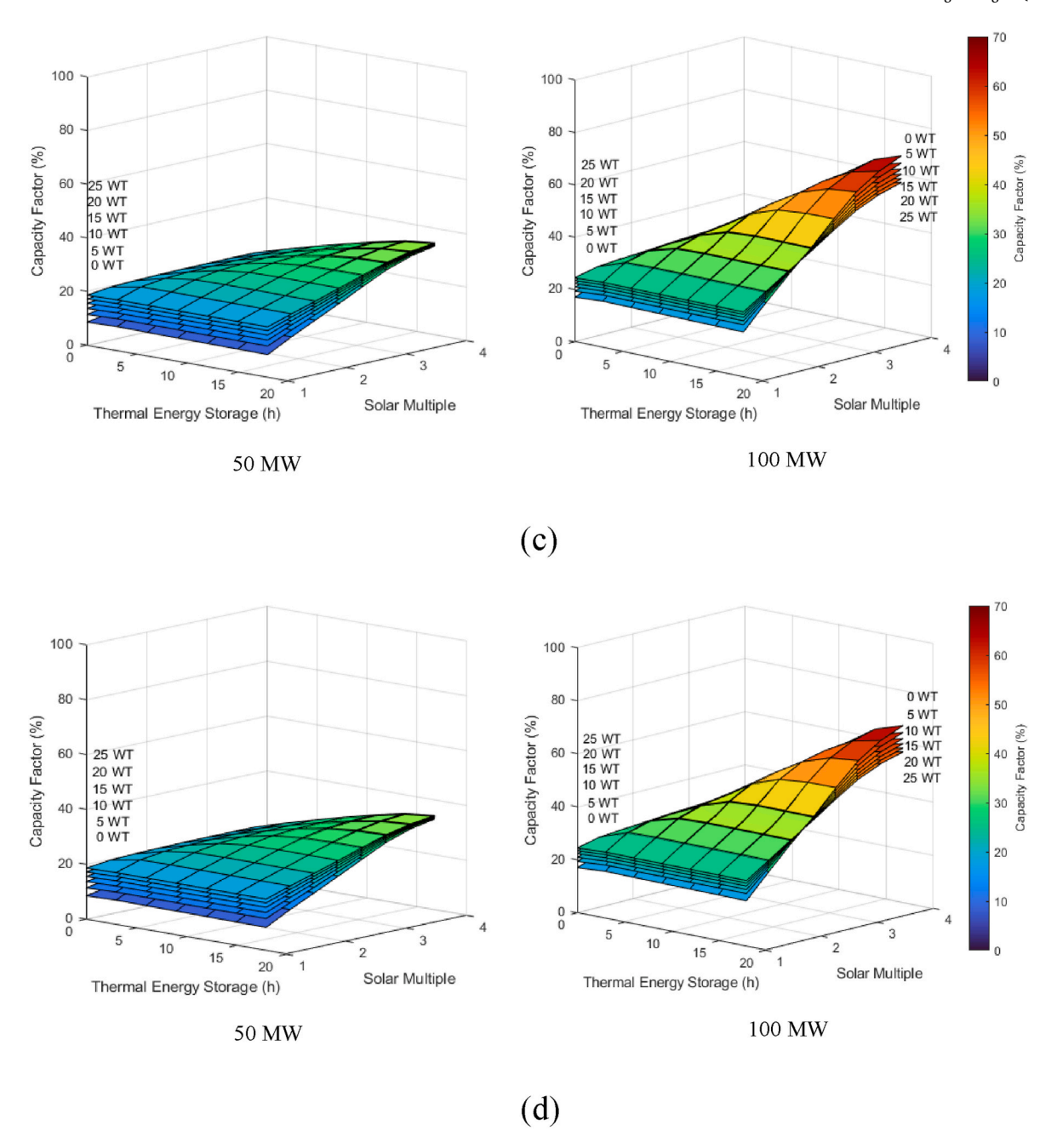


Fig. 11. (continued).

5. Conclusion

The main drive behind this work is the assessment of two of the most important risks to SPT's feasibility in arid regions: aerosols density and water scarcity. To this direction, the study develops and analyses new designs including WT hybridisation aiming at enhancing the performance of SPT and reduce costs.

The aerosols levels have been quantified and integrated into a convenient simulation tool and then the effect of the aerosols inclusion has been tested. For that, one year of ground measured AOD data has been used to site adapt five years long data of MERRA-2 AOD data. Then, the five years site adapted AOD has been represented in a TAY form, from which the yearly AOD average has been integrated in the SAM simulation tool as a yearly aerosols representative value.

The variation of the SPT capacity from 50 to 100 MW has revealed an increasing effect of aerosols on the solar field output. Despite the

noticeable increase, this has not been very sharp as the total loss of the AEG due to the aerosols inclusion reaches a maximum of 9.1 % when the SPT capacity is at 100 MW. This deviation does not disqualify a potential SPT from being feasible, however, it does give a more accurate vision of the plant expected performance as the deviation of the AEG translates to a deviation in the CF, LCOE, etc. On the other hand, this effect of the aerosols can only be minimized by the adoption of smaller solar fields sizes as these have shorter slant ranges, thus the reflected irradiance travelling distance towards the receiver is shorter and the attenuation is lower. That's in addition to the fact that when adopting larger solar fields, the newly configured heliostats are placed at the outer circumference of the already existing ones, i.e. having even larger slant range which is a subject of more aerosols effect.

Regarding the water consumption, four different cooling options have been thoroughly analysed; these include air and water-cooled condensers as well as hybrid condensers of 19 % and 30 % (of wet

M.S. Alfailakawi et al. Results in Engineering 24 (2024) 102968

cooling). For a standalone SPT, the proposed hybrid condenser scenarios exhibit marginally lower AEG but significantly lower water consumption than the water-cooled scenario; and hence the balance of this trade-off appears to favour the hybrid condenser scenarios. The opposite trend has been found when the hybrid condenser scenarios are compared to the air-cooled condenser, in which case both hybrid condenser scenarios result in greater AEG, but, for reasonably more consumed water.

The second main goal of this work is to propose an appropriate design to make up for the AEG loss due to the aerosols intensity. For this, WT integration has been proposed. WT can also contribute in driving the LCOE down, i.e. an important objective function in this work. In addition, as it consumes no water, WT is a suitable hybridization solution for a SPT coupled with TES that both consume water. On the other hand, the proposed WT integration has its own limitation, as for example, the amount of the AEG generated from the WT cannot match the generation of a standalone SPT of the same capacity, since in the current design the WT does not employ any back-up system.

The SPT-WT hybridization has been realized in the SAM environment with the assistance of an in-house developed algorithm that is capable of automating the calculations of the most important indicators of both the SPT and WT individual performance models. The implementation of the in-house algorithm is crucial for the assessments as even if it is not a nested feature of SAM, it can still take advantage of the SAM capabilities in terms of calculating the energy performance of the renewable technologies.

This study has exemplified robust methods for the effective integration of WT with SPT in arid regions. These methods with proper modifications can be also extended to other renewable technologies and to different regions. Finally, based on the modelling results, the proposed energy solution appears to be a very competitive solution for Kuwait (and other regions with similar weather conditions) energy mix

towards decarbonisation and increased reliability.

CRediT authorship contribution statement

Mohammed S. Alfailakawi: Writing – original draft, Validation, Software, Methodology, Investigation, Data curation, Conceptualization. Stavros Michailos: Writing – review & editing, Validation, Supervision, Methodology, Conceptualization. Derek B. Ingham: Writing – review & editing, Supervision, Resources, Project administration. Kevin J. Hughes: Supervision, Resources, Project administration. Lin Ma: Supervision, Resources, Project administration. Mohamed Pourkashanian: Supervision, Resources, Project administration.

Declaration of competing interest

The authors declare that they have no known competing financial interests or personal relationships that could have appeared to influence the work reported in this paper.

Data availability

Data will be made available on request.

Acknowledgements

The authors would like to thank the University of Sheffield Institutional Open Access Fund. For the purpose of open access, the authors have applied a Creative Commons Attribution (CC BY) licence to any Author Accepted Manuscript version arising.

The authors also would like to acknowledge the Kuwait Ministry of Defence for their valuable financial support.

Nomenclature

General	
A	attenuation percentage (%)
A _{hel}	heliostats area (m ²)
N _{hel}	number of heliostats (-)
h	tower height
n	analysis period (year)
S	slant range (m)
T_d	dry bulb temperature (K)
ν	wind speed (m/s)
Z	wind turbine height (m)
Abbreviations	
AEG	annual energy generation
AOD	aerosols optical depth
CAPEX	capital expenditures
CF	capacity factor
CSP	concentrated solar power
DNI	direct normal irradiance
HTF	heat transfer fluid
KISR	Kuwait institute of scientific research
LCOE	levelized cost of energy
LK	language kit
MENA	Middle East North Africa
MS	molten salt
SAM	System advisor model
SM	solar multiple
SPT	solar power tower
TAY	typical aerosol year
TES	thermal energy storage
TMY	typical metrological year
WT	wind turbine
SREP	Shagaya renewable energy park
Subscripts	
P_R	wind rated power
ν_{C}	cut-in speed
v_0	cut-out speed
	(continued on next page)

(continued on next page)

,		7.
	ntinı	

ν_R	rated wind speed
Greek symbols	
α	power law exponent (-)
η_{at}	attenuation loss (%)
η_{cos}	cosine loss (%)
η_d	dry cooled cycle efficiency (%)
η_{opt}	solar field optical efficiency (%)
η_{rec}	spillage loss (%)
$\eta_{sp}\eta_{s\&b}$	receiver efficiency (%)
η_w	shadowing & blocking loss (%)
Q _{Field}	wet cooled cycle efficiency (%)
Q_{HTF}	solar field incident power (kWh)
Q _{rec}	HTF thermal power (kWh)
Q_{TES}	receiver incident power (kWh)
q_{pb}	TES thermal power (kWh)
ϕ	power block thermal power (kWh)
,	relative humidity (%)

Appendix A. Supplementary data

Supplementary data to this article can be found online at https://doi.org/10.1016/j.rineng.2024.102968.

References

- [1] U. Pelay, L. Luo, Y. Fan, D. Stitou, M. Rood, Thermal energy storage systems for concentrated solar power plants, Renew. Sustain. Energy Rev. 79 (2017) 82–100, https://doi.org/10.1016/j.rser.2017.03.139.
- [2] M. Shahabuddin, M.A. Alim, T. Alam, M. Mofijur, S.F. Ahmed, G. Perkins, A critical review on the development and challenges of concentrated solar power technologies, Sustain. Energy Technol. Assessments 47 (2021) 101434, https://doi. org/10.1016/j.seta.2021.101434.
- [3] E. González-Roubaud, D. Pérez-Osorio, C. Prieto, Review of commercial thermal energy storage in concentrated solar power plants: steam vs. molten salts, Renew. Sustain. Energy Rev. 80 (2017) 133–148, https://doi.org/10.1016/j. rser.2017.05.084.
- [4] K. Vignarooban, X. Xu, A. Arvay, K. Hsu, A.M. Kannan, Heat transfer fluids for concentrating solar power systems - a review, Appl. Energy 146 (2015) 383–396, https://doi.org/10.1016/j.apenergy.2015.01.125.
- [5] R.I. Dunn, P.J. Hearps, M.N. Wright, Molten-salt power towers: newly commercial concentrating solar storage, Proc. IEEE 100 (2012) 504–515, https://doi.org/ 10.1109/JPROC.2011.2163739.
- [6] Samaan Ladkany, William Culbreth, Nathan Loyd, Molten salts and applications III: worldwide molten salt technology developments in energy production and storage, J. Energy Power Eng. 12 (2018) 533–544, https://doi.org/10.17265/1934-8975/ 2018-13.002
- [7] S.A. Khalil, A.M. Shaffie, Attenuation of the solar energy by aerosol particles: a review and case study, Renew. Sustain. Energy Rev. 54 (2016) 363–375, https://doi.org/10.1016/j.rser.2015.09.085.
- [8] C.A. Gueymard, Uncertainties in modeled direct irradiance around the sahara as affected by aerosols: are current datasets of bankable quality, J Sol Energy Eng Trans ASME 133 (2011) 1–13, https://doi.org/10.1115/1.4004386.
- [9] C.A. Gueymard, Impact of on-site atmospheric water vapor estimation methods on the accuracy of local solar irradiance predictions, Sol. Energy 101 (2014) 74–82, https://doi.org/10.1016/j.solener.2013.12.027.
- [10] E. Mielke, L. Diaz Anadon, V. Narayanamurti, Water consumption of energy resource extraction, processing, and conversion, Harvard Kennedy Sch Energy Technol Innov Policy Discuss Pap Ser 52 (2010).
- [11] S. Bouaddi, A. Fernández-García, C. Sansom, J.A. Sarasua, F. Wolfertstetter, H. Bouzekri, et al., A review of conventional and innovative- sustainable methods for cleaning reflectors in concentrating solar power plants, Sustain. Times 10 (2018), https://doi.org/10.3390/su10113937.
- [12] Water's High Heat Capacity n.d. https://bio.libretexts.org/Bookshelves/ Introductory_and_General_Biology/Book%3A_General_Biology_(Boundless)/2%3A_ The Chemical_Foundation_of_Life/2.2%3A_Water/2.2C%3A_Water's_High_Heat_ Capacity (accessed September 2, 2020).
- [13] The Heat Capacity of Air is too Low to Heat Oceans of Melt Polar Ice n.d. htt p://nov79.com/gbwm/htcap.html (accessed September 2, 2020).
- [14] S. Zafar, Water scarcity in MENA 2024. https://www.ecomena.org/water-scarcity-in-mena/. (Accessed 3 September 2024).
- [15] Vittitoe CN, Biggs F. TERRESTRIAL PROPAGATION LOSS 1978.
- [16] N. Hanrieder, S. Wilbert, D. Mancera-Guevara, R. Buck, S. Giuliano, R. Pitz-Paal, Atmospheric extinction in solar tower plants – a review, Sol. Energy 152 (2017) 193–207, https://doi.org/10.1016/j.solener.2017.01.013.
- [17] C.L. Pitman, L.L. Vant-Hull, Atmospheric transmittance model for a solar beam propagating between a heliostat and a receiver, ASES Prog Sol Energy (1982) 1247–1251.

- [18] J. Ballestrín, A. Marzo, Solar radiation attenuation in solar tower plants, Sol. Energy 86 (2012) 388–392, https://doi.org/10.1016/j.solener.2011.10.010.
- [19] E. Carra, J. Ballestrín, J. Polo, J. Barbero, J. Fernández-Reche, Atmospheric extinction levels of solar radiation at Plataforma Solar de Almería. Application to solar thermal electric plants, Energy 145 (2018) 400–407, https://doi.org/ 10.1016/j.energy.2017.12.111.
- [20] J. Polo, J. Ballestrín, E. Carra, Sensitivity study for modelling atmospheric attenuation of solar radiation with radiative transfer models and the impact in solar tower plant production, Sol. Energy 134 (2016) 219–227, https://doi.org/ 10.1016/j.solener.2016.04.050.
- [21] J. Polo, J. Ballestrín, J. Alonso-Montesinos, G. López-Rodriguez, J. Barbero, E. Carra, et al., Analysis of solar tower plant performance influenced by atmospheric attenuation at different temporal resolutions related to aerosol optical depth, Sol. Energy 157 (2017) 803–810, https://doi.org/10.1016/j. solener.2017.09.003.
- [22] A. Rouibah, D. Benazzouz, R. Kouider, A. Al-Kassir, J. García-Sanz-Calcedo, K. Maghzili, Solar tower power plants of molten salt external receivers in Algeria: analysis of direct normal irradiation on performance, Appl. Sci. 8 (2018), https://doi.org/10.3390/app8081221.
- [23] S. Boudaoud, A. Khellaf, K. Mohammedi, O. Behar, Thermal performance prediction and sensitivity analysis for future deployment of molten salt cavity receiver solar power plants in Algeria, Energy Convers. Manag. 89 (2015) 655–664, https://doi.org/10.1016/j.enconman.2014.10.033.
- [24] S. Mihoub, A. Chermiti, H. Beltagy, Methodology of determining the optimum performances of future concentrating solar thermal power plants in Algeria, Energy 122 (2017) 801–810, https://doi.org/10.1016/j.energy.2016.12.056.
- [25] H. Murat Cekirge, A comparison of solar power systems (CSP): solar tower (ST) systems versus parabolic trough (PT) systems, Am. J. Energy Eng. 3 (2015) 29, https://doi.org/10.11648/j.ajee.20150303.11.
- [26] K. Hirbodi, M. Enjavi-Arsanjani, M. Yaghoubi, Techno-economic assessment and environmental impact of concentrating solar power plants in Iran, Renew. Sustain. Energy Rev. 120 (2020), https://doi.org/10.1016/j.rser.2019.109642.
- [27] M.S. Alfailakawi, S. Michailos, D.B. Ingham, K.J. Hughes, L. Ma, M. Pourkashanian, Multi-temporal resolution aerosols impacted techno-economic assessment of concentrated solar power in arid regions: case study of solar power tower in Kuwait, Sustain. Energy Technol. Assessments 52 (2022) 102324, https://doi.org/ 10.1016/j.seta.2022.102324.
- [28] F.J. Santos-Alamillos, D. Pozo-Vázquez, J.A. Ruiz-Arias, L. Von Bremen, J. Tovar-Pescador, Combining wind farms with concentrating solar plants to provide stable renewable power, Renew. Energy 76 (2015) 539–550, https://doi.org/10.1016/j.renene.2014.11.055.
- [29] S. Pramanik, R.V. Ravikrishna, A review of concentrated solar power hybrid technologies, Appl. Therm. Eng. 127 (2017) 602–637, https://doi.org/10.1016/j. applthermaleng.2017.08.038.
- [30] A.Z. Sahin, Applicability of wind-solar thermal hybrid power systems in the northeastern part of the Arabian Peninsula, Energy Sources 22 (2000) 845–850, https://doi.org/10.1080/009083100300001645.
- [31] C. Kost, B. Pfluger, W. Eichhammer, M. Ragwitz, Fruitful symbiosis: why an export bundled with wind energy is the most feasible option for North African concentrated solar power, Energy Pol. 39 (2011) 7136–7145, https://doi.org/ 10.1016/j.enpol.2011.08.032
- [32] R. Sioshansi, P. Denholm, Benefits of colocating concentrating solar power and wind, IEEE Trans. Sustain. Energy 4 (2013) 877–885, https://doi.org/10.1109/ TSTE.2013.2253619.

- [33] B.D. Vick, T.A. Moss, Adding concentrated solar power plants to wind farms to achieve a good utility electrical load match, Sol. Energy 92 (2013) 298–312, https://doi.org/10.1016/j.solener.2013.03.007.
- [34] M. Al-Addous, M. Bdour, S. Rabaiah, A. Boubakri, N. Schweimanns, N. Barbana, et al., Innovations in solar-powered desalination: a comprehensive review of sustainable solutions for water scarcity in the Middle East and North Africa (MENA) region, Water (Switzerland) 16 (2024), https://doi.org/10.3390/wi6131877.
- [35] M. Hejazi, S.R. Santos Da Silva, F. Miralles-Wilhelm, S. Kim, P. Kyle, Y. Liu, et al., Impacts of water scarcity on agricultural production and electricity generation in the Middle East and North Africa, Front. Environ. Sci. 11 (2023) 1–16, https://doi. org/10.3389/fenvs.2023.1082930.
- [36] A.M. Blanco-Marigorta, M. Victoria Sanchez-Henríquez, J.A. Peña-Quintana, Exergetic comparison of two different cooling technologies for the power cycle of a thermal power plant, Energy 36 (2011) 1966–1972, https://doi.org/10.1016/j. energy 2010.09.033
- [37] MS Ben Fares, S. Abderafi, Water consumption analysis of Moroccan concentrating solar power station, Sol. Energy 172 (2018) 146–151, https://doi.org/10.1016/j. solarger 2018 06 003
- [38] C.S. Turchi, M.J. Wagner, C.F. Kutscher, Water use in parabolic trough CSPsummary results from worley parsons' analyses. https://doi.org/10.2172/1001357 2010
- [39] A. Poullikkas, I. Hadjipaschalis, G. Kourtis, A comparative overview of wet and dry cooling systems for Rankine cycle based CSP plants, Trends Heat Mass Transf 13 (2012) 377-50.
- [40] F. Asfand, P. Palenzuela, L. Roca, A. Caron, C.A. Lemarié, J. Gillard, et al., Thermodynamic performance and water consumption of hybrid cooling system configurations for concentrated solar power plants, Sustain. Times 12 (2020), https://doi.org/10.3390/su12114739.
- [41] M.J. Wagner, C. Kutscher, The impact of hybrid wet/dry cooling on concentrating solar power plant performance, Proc. ASME 2010 4th Int. Conf. Energy Sustain. (2010) 1–8, https://doi.org/10.1115/ES2010-90442.
- [42] S. El Marazgioui, A. El Fadar, Impact of cooling tower technology on performance and cost-effectiveness of CSP plants, Energy Convers. Manag. 258 (2022) 115448, https://doi.org/10.1016/j.enconman.2022.115448.
- [43] B.N. Holben, T.F. Eck, I. Slutsker, D. Tanré, J.P. Buis, A. Setzer, et al., Aeronet a federated instrument network and data archive for aerosol characterization, Remote Sens. Environ. 66 (1998) 1–16, https://doi.org/10.1016/S0034-4257(98) 00031-5
- [44] J. Polo, C. Fernández-Peruchena, M. Gastón, Analysis on the long-term relationship between DNI and CSP yield production for different technologies, Sol. Energy 155 (2017) 1121–1129. https://doi.org/10.1016/j.solener.2017.07.059.
- [45] PVGIS PHOTOVOLTAIC GEOGRAPHICAL INFORMATION SYSTEM n.d https://re. jrc.ec.europa.eu/pvg tools/en/.
- [46] N. Blair, A.P. Dobos, J. Freeman, T. Neises, M. Wagner, T. Ferguson, et al., System advisor model, SAM 2014 .1.14: general description. https://doi.org/10.217 2/1126294. 2014.
- [47] A.B. Awan, K.V.V. Chandra Mouli, M. Zubair, Performance enhancement of solar tower power plant: a multi-objective optimization approach, Energy Convers. Manag. 225 (2020) 113378, https://doi.org/10.1016/j.enconman.2020.113378.
- [48] E.B. Agyekum, V.I. Velkin, Optimization and techno-economic assessment of concentrated solar power (CSP) in South-Western Africa: a case study on Ghana, Sustain. Energy Technol. Assessments 40 (2020) 100763, https://doi.org/ 10.1016/j.seta.2020.100763.
- [49] A. Gamil, S.I.U. Gilani, H.H. Al-kayiem, Simulation of incident solar power input to fixed target of central receiver system in Malaysia, IEEE Conf Sustain Util Dev Eng Technol (2013) 92–97, https://doi.org/10.1109/CSUDET.2013.6739506, 2013.
- Technol (2013) 92–97, https://doi.org/10.1109/CSUDET.2013.6739506, 2013.
 [50] M. Saghaffar, K. Mohammadi, K. Powell, Design and analysis of a dual-receiver direct steam generator solar power tower plant with a flexible heliostat field, Sustain. Energy Technol. Assessments 39 (2020) 100698, https://doi.org/10.1016/j.seta.2020.100698.
- [51] A. Izadi, P. Ahmadi, S. Bashiri Mousavi, I. Fakhari, A comparative optimization of a trigeneration system with an innovative integration of solar Heliostat towers and Hydrogen production unit, Sustain. Energy Technol. Assessments 47 (2021) 101522, https://doi.org/10.1016/j.seta.2021.101522.
- [52] E.M.A. Mokheimer, Y.N. Dabwan, M.A. Habib, Optimal integration of solar energy with fossil fuel gas turbine cogeneration plants using three different CSP technologies in Saudi Arabia, Appl. Energy 185 (2017) 1268–1280, https://doi. org/10.1016/j.apenergy.2015.12.029.
- [53] G. Srilakshmi, N.S. Suresh, N.C. Thirumalai, M.A. Ramaswamy, A novel approach to determine the non-dimensional heliostat field boundary for solar tower plants, Sustain. Energy Technol. Assessments 17 (2016) 26–37, https://doi.org/10.1016/j. seta.2016.08.001.

- [54] A.B. Awan, M. Zubair, K.V.V. Chandra Mouli, Design, optimization and performance comparison of solar tower and photovoltaic power plants, Energy 199 (2020) 117450, https://doi.org/10.1016/j.energy.2020.117450.
- [55] Z. Zhao, M.T. Arif, A.M.T. Oo, Solar thermal energy with molten-salt storage for residential heating application, Energy Proc. 110 (2017) 243–249, https://doi.org/ 10.1016/j.egypro.2017.03.134.
- [56] U.S. Department of Energy, Concentrating solar power commercial application study: Reducing water consumption of concentrating solar power electricity generation 2001 (2010), https://doi.org/10.2172/1218186.
- [57] H. Deng, R.F. Boehm, An estimation of the performance limits and improvement of dry cooling on trough solar thermal plants, Appl. Energy 88 (2011) 216–223, https://doi.org/10.1016/j.apenergy.2010.05.027.
- [58] P. Gilman, A. Dobos, System advisor model, SAM 2011.12.2: general description. https://dx.doi.org/10.2172/1046896, 2012.
- [59] C. Marugán-Cruz, S. Sánchez-Delgado, J. Gómez-Hernández, D. Santana, Towards zero water consumption in solar tower power plants, Appl. Therm. Eng. 178 (2020) 115505, https://doi.org/10.1016/j.applthermaleng.2020.115505.
- [60] "Gemasolar" Torresol Energy n.d https://torresolenergy.com/en/gemasolar /(accessed February 28, 2020).
- [61] Mengal Soomro, Khan Memon, Mirjat Shafiq, Performance and economic analysis of concentrated solar power generation for Pakistan, Processes 7 (2019) 575, https://doi.org/10.3390/pr7090575.
- [62] Siemens Gamesa G97 n.d https://en.wind-turbine-models.com/turbines/764-game sa-g97.
- [63] H.Z. Al Garni, A. Abubakar Mas'ud, M.A. Baseer, M.A.M. Ramli, Techno-economic optimization and sensitivity analysis of a PV/Wind/diesel/battery system in Saudi Arabia using a combined dispatch strategy, Sustain. Energy Technol. Assessments 53 (2022) 102730, https://doi.org/10.1016/j.seta.2022.102730.
- [64] M. Al-Rasheedi, M. Al-Khayat, C.A. Gueymard, Haupt S. Ellen, B. Kosović, A. Al-Qattan, et al., Performance analysis of a 10-MW wind farm in a hot and dusty desert environment. Part 1: wind resource and power generation evaluation, Sustain. Energy Technol. Assessments 47 (2021), https://doi.org/10.1016/j.seta.2021.101487.
- [65] J.F. Manwell, J.G. Mcgowan, A.L. Rogers, Wind Energy Explained Theory, Design and Application, second ed., WILEY, 2009 https://doi.org/10.1002/ 9781119994367
- [66] N. Blair, N. Diorio, J. Freeman, P. Gilman, S. Janzou, T. Neises, et al., System advisor model (SAM) general description, Version 2017.9.5, 2018. https://doi. org/10.2172/1440404.
- [67] S. Lude, T.P. Fluri, S. Alhajraf, V. Jülch, P. Kühn, A. Marful, et al., Optimization of the technology mix for the shagaya 2 GW renewable energy Park in Kuwait, Energy Proc. 69 (2015) 1633–1642, https://doi.org/10.1016/j.egypro.2015.03.120.
- [68] NREL, System Advisor Model Help System, 2019.
- [69] Mohammed S. Alfailakawi, Stavros Michailos, Derek B. Ingham, AL-Arfi Ismail, Kevin J. Hughes, Ma MP. Lin, Performance improvement of aerosols impacted concentrated solar power in arid regions, Case Study of Solar Power Tower Hybridization With Wind Turbines in Kuwait (2022), https://doi.org/10.46855/ energy-proceedings-10201.
- [70] G. Rinaldi, A. Garcia-Teruel, H. Jeffrey, P.R. Thies, L. Johanning, Incorporating stochastic operation and maintenance models into the techno-economic analysis of floating offshore wind farms, Appl. Energy 301 (2021) 117420, https://doi.org/ 10.1016/j.apenergy.2021.117420.
- [71] S. Shawki, Kuwait Corporate Taxes on corporate income n.d. https://taxsummaries.pwc.com/kuwait/corporate/taxes-on-corporate-income. (Accessed 26 January 2023).
- [72] J. de la Hoz, H. Martín, J. Miret, M. Castilla, R. Guzman, Evaluating the 2014 retroactive regulatory framework applied to the grid connected PV systems in Spain, Appl. Energy 170 (2016) 329–344, https://doi.org/10.1016/j. apenergy.2016.02.092.
- [73] C.S. Turchi, M. Boyd, D. Kesseli, P. Kurup, M. Mehos, T. Neises, et al., CSP systems analysis - final project. https://doi.org/10.2172/1513197, 2019.
- [74] U.S. Department of Energy, Distributed wind market report. https://doi.org/10. 2172/1220282, 2013.
- [75] Report A, Annual Report of the fiscal year 2020/2021. https://www.cbk.gov.kw/en/statistics-and-publication/publications/annual-reports, 2021 (accessed January 24, 2023).
- [76] Central Bank of Kuwait, CBK raises the discount rate by a half percentage point 2022. https://www.cbk.gov.kw/en/cbk-news/announcements-and-press-release s/press-releases/2022/12/202212061624-cbk-raises-the-discount-rate-by-a-half--percentage-point#:--:text=TheBoardofDirectorsof,%25effectiveDecember7% 2C2022. (Accessed 24 January 2023).
- [77] Kuwait short term interest rate 2022. https://www.ceicdata.com/en/indicator/kuwait/short-term-interest-rate#:~:text=KuwaitShortTermInterestRate%3AMonth End%3AKIBOR%3A3. (Accessed 18 January 2023). Nov 2001 to Dec 2022.